JCB Journal of Cell Biology

ARTICLE

The ER cholesterol sensor SCAP promotes CARTS biogenesis at ER–Golgi membrane contact sites

Yuichi Wakana[1], Kaito Hayashi[1]*, Takumi Nemoto[1]*, Chiaki Watanabe[1], Masato Taoka[2], Jessica Angulo-Capel[3], Maria F. Garcia-Parajo[3,4], Hidetoshi Kumata[1], Tomonari Umemura[1], Hiroki Inoue[1], Kohei Arasaki[1], Felix Campelo[3], and Mitsuo Tagaya[1]

In response to cholesterol deprivation, SCAP escorts SREBP transcription factors from the endoplasmic reticulum to the Golgi complex for their proteolytic activation, leading to gene expression for cholesterol synthesis and uptake. Here, we show that in cholesterol-fed cells, ER-localized SCAP interacts through Sac1 phosphatidylinositol 4-phosphate (PI4P) phosphatase with a VAP–OSBP complex, which mediates counter-transport of ER cholesterol and Golgi PI4P at ER–Golgi membrane contact sites (MCSs). SCAP knockdown inhibited the turnover of PI4P, perhaps due to a cholesterol transport defect, and altered the subcellular distribution of the VAP–OSBP complex. As in the case of perturbation of lipid transfer complexes at ER–Golgi MCSs, SCAP knockdown inhibited the biogenesis of the trans-Golgi network–derived transport carriers CARTS, which was reversed by expression of wild-type SCAP or a Golgi transport–defective mutant, but not of cholesterol sensing–defective mutants. Altogether, our findings reveal a new role for SCAP under cholesterol-fed conditions in the facilitation of CARTS biogenesis via ER–Golgi MCSs, depending on the ER cholesterol.

Introduction

Cholesterol and sphingolipids can form liquid-ordered membrane nanodomains that are segregated from other lipids and thus are proposed to serve as platforms for specific proteins that regulate signal transduction and endocytosis at the plasma membrane (PM) and apical transport from the TGN (Keller and Simons, 1998; Klemm et al., 2009; Simons and Sampaio, 2011; Jacobson et al., 2019). Increasing evidence—including recent experiments in which sphingomyelin (SM) metabolism at the trans-Golgi membranes was perturbed—strongly suggests that such lipid nanodomains are required for the functional organization of enzymatic domains, cargo sorting, and transport carrier biogenesis at the TGN (Duran et al., 2012; van Galen et al., 2014; Deng et al., 2016; Campelo et al., 2017; Capasso et al., 2017; Deng et al., 2018) and thereby are crucial to maintain homeostatic control of the Golgi function.

De novo biosynthesis of cholesterol occurs at the ER, where a key regulatory protein in cholesterol metabolism called sterol regulatory element–binding protein (SREBP) cleavage-activating protein (SCAP) localizes. SCAP is a polytopic membrane protein that functions as an ER cholesterol sensor to control the cellular cholesterol content (Hua et al., 1996; Brown et al., 2018). When the ER cholesterol level is low, SCAP escorts the membrane-bound transcription factors SREBPs into COPII vesicles for their export from the ER to the Golgi complex. There, SREBPs are cleaved by proteases, allowing their transcriptionally active domain to enter the nucleus and promote expression of genes involved in cholesterol synthesis and uptake. Conversely, when cholesterol in the ER membrane is abundant, cholesterol binds to SCAP and triggers conformational changes that allow SCAP to interact with the integral ER membrane protein Insig, which retains SCAP in the ER along with unprocessed SREBPs. Other than sequestering SREBPs at the ER, however, it remains unclear whether SCAP has functions under cholesterol-fed conditions.

Although the ER produces cholesterol and also receives it from the PM and other sources, ER cholesterol content is low (Ikonen, 2018). This is accomplished through the export of cholesterol from the ER against the concentration gradient in both vesicular and nonvesicular manners, the latter of which occurs at membrane contact sites (MCSs). In particular, at ER–Golgi MCSs, Golgi-associated oxysterol-binding protein (OSBP) interacts with an integral ER membrane protein named vesicle-associated membrane protein–associated protein (VAP) to transfer cholesterol from the ER to the trans-Golgi membranes,

[1]School of Life Sciences, Tokyo University of Pharmacy and Life Sciences, Hachioji, Tokyo, Japan; [2]Faculty of Science, Department of Chemistry, Tokyo Metropolitan University, Hachioji, Tokyo, Japan; [3]Institut de Ciencies Fotoniques, The Barcelona Institute of Science and Technology, Barcelona, Spain; [4]Institució Catalana de Recerca i Estudis Avançats, Barcelona, Spain.

*K. Hayashi and T. Nemoto contributed equally to this paper; Correspondence to Yuichi Wakana: ywakana@toyaku.ac.jp; Mitsuo Tagaya: tagaya@toyaku.ac.jp.

© 2020 Wakana et al. This article is distributed under the terms of an Attribution–Noncommercial–Share Alike–No Mirror Sites license for the first six months after the publication date (see http://www.rupress.org/terms/). After six months it is available under a Creative Commons License (Attribution–Noncommercial–Share Alike 4.0 International license, as described at https://creativecommons.org/licenses/by-nc-sa/4.0/).

Downloaded from http://rupress.org/jcb/article-pdf/220/1/e202002150/1617891/jcb_202002150.pdf by guest on 06 May 2026

accompanied by reciprocal transfer of phosphatidylinositol 4-phosphate (PI4P; Mesmin et al., 2013). PI4P transported to the ER is hydrolyzed by the ER-localized lipid phosphatase Sac1, which thus seems to provide a driving force for cholesterol transport (Antonny et al., 2018; Zewe et al., 2018).

ER–Golgi MCSs also control the transport of ceramide from the ER to the trans-Golgi membranes. This nonvesicular transport is mediated by a complex of VAP and ceramide transfer protein (CERT) and leads to the biosynthesis of SM and DAG by SM synthase at the trans-Golgi membranes (Hanada et al., 2003; Kawano et al., 2006). Importantly, PI4P in the trans-Golgi membranes is crucial for both OSBP and CERT to associate with the Golgi complex (De Matteis et al., 2005), and, hence, the biosynthesis and metabolism of cholesterol, SM, PI4P, and DAG are either directly or indirectly interconnected (Kumagai and Hanada, 2019). Of note, DAG recruits to the TGN a serine/threonine kinase, PKD, which phosphorylates CERT and OSBP to release these proteins from the Golgi complex (Baron and Malhotra, 2002; Fugmann et al., 2007; Nhek et al., 2010). PKD kinase activity also contributes to the membrane fission reaction required for transport carrier biogenesis at the TGN (Liljedahl et al., 2001; Malhotra and Campelo, 2011; Pagliuso et al., 2016).

On the basis of these reports and our previous data, we proposed a model in which lipid transfer at ER–Golgi MCSs promotes the biogenesis of carriers of the TGN to the cell surface (CARTS; Wakana et al., 2015), which transport selective cargoes from the TGN to the PM (Wakana et al., 2012, 2013). In this context, lipid transfer at these MCSs needs to be strictly controlled on demand for TGN-to-PM transport, but the molecular mechanisms underlying this regulation remain largely elusive. In this study, we identified SCAP as a novel Sac1-interacting protein at ER–Golgi MCSs. Our data show a new function of SCAP under cholesterol-fed conditions, in which SCAP interacts with the cholesterol/PI4P exchange machinery at ER–Golgi MCSs and facilitates the biogenesis of CARTS in an ER cholesterol–dependent manner.

Results

Identification of SCAP as a novel component of Sac1-positive ER–Golgi MCSs

We previously reported that the perinuclear Sac1 localization represents its presence at specialized ER subdomains that are closely apposed to the TGN membranes, most likely corresponding to ER–Golgi MCSs, rather than at the Golgi complex (Wakana et al., 2015). To identify novel components of ER–Golgi MCSs, we explored Sac1-interacting proteins using a Sac1 K2A mutant (Blagoveshchenskaya et al., 2008; Dippold et al., 2009), which is more highly enriched in the juxtanuclear region than the WT protein, as revealed by its reduced peripheral staining (Fig. 1 A). This mutant has replacement of two lysines in the C-terminal COPI-interacting motif with alanines. While the dilysine COPI-interacting motif is used for retrograde transport from the cis-Golgi to the ER (Gomez-Navarro and Miller, 2016), some ER integral membrane proteins also use this signal for their movement along the ER from the cell center to the periphery (Wakana et al., 2008; Lavieu et al., 2010).

The deconvolved, enhanced-contrast, and increased-resolution images of cells treated with 25-hydroxycholesterol (25-HC), a reagent that binds to OSBP and promotes the targeting of the VAP–OSBP complex to ER–Golgi MCSs (Ridgway et al., 1992; Suchanek et al., 2007; Mesmin et al., 2013), showed good overlap between the GFP-Sac1 K2A signal and that of the integral ER membrane protein VAP-A and also the close apposition, but not full overlap, of GFP-Sac1 K2A to the TGN marker TGN46, similarly to WT (Fig. 1 B). To more clearly distinguish between ER–Golgi MCSs and the Golgi membranes, we further treated cells with the microtubule-depolymerizing agent nocodazole, which induces the formation of dispersed Golgi ministacks in the cytoplasm (Cole et al., 1996). Consequently, colocalization of GFP-Sac1–positive small punctate elements with VAP-A (Fig. S1 A, arrowheads) was observed, but not with the control ER marker Bap31 (Fig. S1 B) and only partially with TGN46 (Fig. S1 C). Although previous work reported that GFP-Sac1 localizes to the cis-Golgi membranes (Liu et al., 2008; Cheong et al., 2010), the colocalization with the cis-Golgi marker GM130 was limited both in the presence and in the absence of nocodazole (Fig. S1). Consistently, the continuity of GFP-Sac1 K2A-positive juxtanuclear membrane compartments with the peripheral ER membrane was demonstrated by inverse FRAP (iFRAP; Fig. 1 C): photobleaching of the peripheral area immediately decreased the perinuclear signals of GFP-Sac1 WT and K2A, but not of the Golgi resident protein N-acetylglucosaminyl transferase I–GFP (NA-GFP). These results suggest that the Sac1 K2A mutant is prominently localized to ER–Golgi MCSs and validate the use of this mutant as a bait to identify interacting proteins at the MCSs.

Immunoprecipitation of FLAG-tagged Sac1 K2A followed by mass spectrometry (MS) analysis revealed multiple interactors of FLAG-Sac1 K2A (Fig. 1 D, lane 2) with decreased binding of COPI coat proteins, which are major interactors for FLAG-Sac1 WT (Fig. 1 D, lane 1, asterisks). The identified Sac1 K2A–interacting proteins include known components of ER–Golgi MCSs such as VAP-A, VAP-B, and OSBP, together with proteins with unknown functions at the MCSs, including SCAP (Fig. 1 E). As shown in Fig. 1 F, immunoprecipitation with an anti-Sac1 antibody revealed a specific interaction of SCAP with endogenous Sac1. Here, we focus on SCAP because, although it had been previously shown to interact with VAP-A and VAP-B, the physiological role of this interaction remains unexplored (Yang et al., 2002).

ER-localized SCAP interacts through Sac1 with the VAP-A–OSBP complex at ER–Golgi MCSs

To confirm that SCAP is a bona fide component of ER–Golgi MCSs, the interactions of FLAG-tagged hamster SCAP with VAP-A, OSBP, and Sac1 were examined by immunoprecipitation (Fig. 2 A). Endogenous Sac1 and VAP-A were clearly coprecipitated with FLAG-SCAP, but not with the FLAG vector control (Fig. 2 A, lanes 7 and 9). When Myc-OSBP was coexpressed, this protein was coprecipitated with FLAG-SCAP, and the interaction of FLAG-SCAP with VAP-A, but not with Sac1, was enhanced (Fig. 2 A, lanes 9 and 10). For negative controls, we showed that an integral ER membrane protein, reticulon-4B (RTN-4B), and another lipid

Downloaded from http://rupress.org/jcb/article-pdf/220/1/e202002150/1617891/jcb_202002150.pdf by guest on 06 May 2026

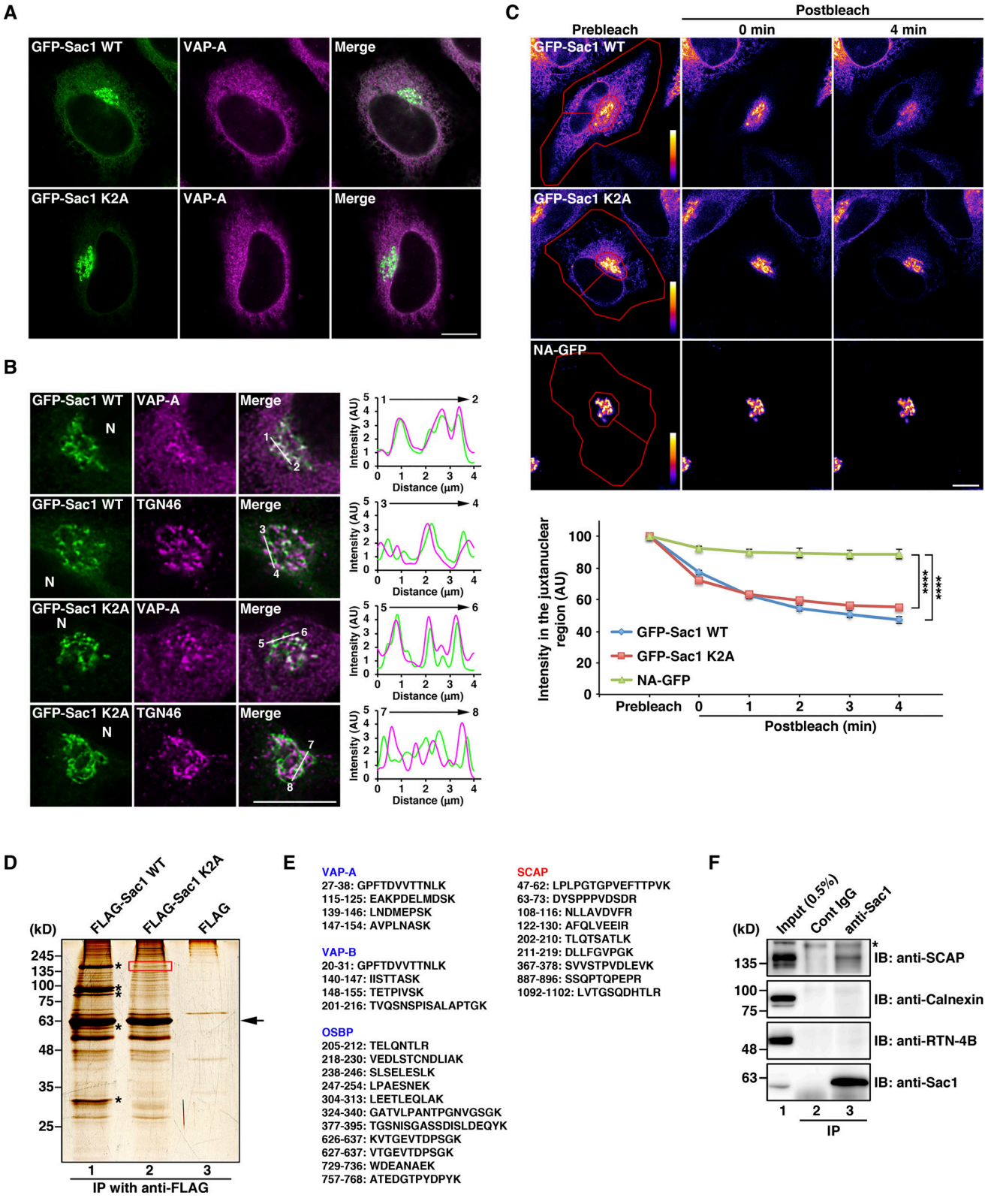

Figure 1. **Identification of SCAP as a novel component of Sac1-positive ER–Golgi MCSs. (A)** Juxtanuclear localization of the GFP-Sac1 WT and K2A mutant in HeLa cells. **(B)** Colocalization of GFP-Sac1 WT or K2A with VAP-A and their proximity to TGN46. HeLa cells expressing GFP-Sac1 WT or K2A were treated with 2 µg/ml 25-HC for 1 h. Images were subjected to deconvolution processing as described in Materials and methods. The graphs on the right show the fluorescence intensity of GFP-Sac1 WT or K2A (green), and VAP-A or TGN46 (magenta) along the respective white lines shown in the merged images. N, nucleus. **(C)** iFRAP in HeLa cells expressing GFP-Sac1 WT, K2A, or NA-GFP. The areas delimited by a red line were bleached as described in Materials and methods. The graph shows quantification of the fluorescence intensity of the indicated proteins in the nonbleached, juxtanuclear region. Data are means ± SEM (n = 4 cells per condition; ****, $P < 0.0001$; one-way ANOVA multiple comparison test). **(D)** Silver staining of immunoprecipitated proteins with FLAG-Sac1 WT,

Downloaded from http://rupress.org/jcb/article-pdf/220/1/e202002150/1617891/jcb_202002150.pdf by guest on 06 May 2026

FLAG-Sac1 K2A, or FLAG in HEK 293T cells. The arrow indicates FLAG-Sac1. Asterisks denote protein bands containing COPI components. SCAP was identified in the protein band boxed with a red line. **(E)** Peptides of VAP-A, VAP-B, OSBP, and SCAP, which were identified by MS analysis of FLAG-Sac1 K2A immunoprecipitates (lane 2 in D). **(F)** Interaction of endogenous Sac1 with SCAP, but not with calnexin or RTN-4B. HEK 293T cell lysate was incubated with Dynabeads Protein G coupled with control (Cont) IgG or an anti-Sac1 antibody, and the cell lysate (Input) and immunoprecipitates (IPs) were immunoblotted (IB) with the indicated antibodies. Asterisk denotes nonspecific bands. Scale bars, 10 µm. AU, arbitrary units.

transfer protein, CERT, were not coprecipitated with FLAG-SCAP (Fig. 2 B).

Next, we asked whether SCAP interacts with the VAP-A–OSBP complex via Sac1. Our previous work showed that Sac1 interacts with VAP-A via OSBP (Wakana et al., 2015). We used two OSBP mutants, FF/AA (Wyles et al., 2002; Loewen et al., 2003) and PH-FFAT (Mesmin et al., 2013), that are defective in binding to VAP and Sac1, respectively (Fig. 2 A, bottom; and Fig. 2 C). In cells expressing Myc-OSBP FF/AA, this protein, but not VAP-A, was found to interact with FLAG-SCAP (Fig. 2 A, lane 11), suggesting that VAP-A is not needed for the interaction of SCAP with OSBP. By contrast, Myc-OSBP PH-FFAT did not coprecipitate with FLAG-SCAP (Fig. 2 A, lane 12). Although previous work revealed that Myc-OSBP PH-FFAT fixes and expands ER–Golgi MCSs through its stable interaction with VAP-A (Mesmin et al., 2013), it inhibited the interaction of FLAG-Sac1 with VAP-A (Fig. 2 C, lane 12). Myc-OSBP PH-FFAT defective in Sac1 binding also greatly reduced the interaction of FLAG-SCAP with VAP-A (Fig. 2 A, lane 12), emphasizing the requirement of Sac1 for the interaction of SCAP with the VAP-A–OSBP complex. Similar results were obtained for a FLAG-tagged C-terminal cytoplasmic fragment (C-term) of SCAP that includes WD (tryptophan–aspartate) repeats (Fig. 2 D). The specific interaction between FLAG-SCAP and Sac1 was also detected in HeLa cells stably expressing FLAG-SCAP at a level of about four times the level of endogenous SCAP (Fig. 2, E and F). These results exclude the possibility of membrane aggregation or cosedimentation with FLAG-SCAP. The specific but relatively weak interactions of SCAP with the cholesterol/PI4P exchange machinery most likely reflect transient interactions among these components, consistent with the underlying association–dissociation dynamics of ER–Golgi contacts that are crucial for their function (Mesmin et al., 2013; Wakana et al., 2015).

To corroborate that ER-localized SCAP, but not Golgi-localized SCAP, can form a complex with VAP-A, OSBP, and Sac1 at ER–Golgi MCSs, we used a SCAP mutant with replacement of aspartic acid 451 and leucine 452 with alanines at the MELADL motif in loop 6 (D451A/L452A), which is defective in COPII binding and therefore cannot exit the ER in COPII-coated vesicles (Sun et al., 2005). FLAG-SCAP D451A/L452A showed interactions with VAP-A, OSBP, and Sac1, analogous to FLAG-SCAP WT (Fig. 2 G).

We next visualized the interactions of SCAP with these proteins in intact cells by using bimolecular fluorescence complementation (BiFC). As shown previously (Kentala et al., 2015; Weber-Boyvat et al., 2015), a BiFC signal derived from the interaction between Vn (N-terminal fragment of Venus)-fused OSBP and Vc (C-terminal fragment of Venus)-fused VAP-A was detected at the perinuclear region representing ER–Golgi MCSs (Fig. S2 C, top row), whereas no signal was detected when only Vn- or Vc-fused constructs were individually expressed (Fig. S2, A and B). This signal was enhanced by 25-HC treatment (Fig. S2 C, middle row). Similar results were obtained with the combination of Vn-OSBP–Vc-Sac1 (Fig. S2 D). The Vn-SCAP–Vc-Sac1 and Vn-SCAP–Vc-VAP-A interactions were also observed upon coexpression of Myc-OSBP, and these interactions were enhanced by 25-HC treatment (Fig. 3, A–D). These BiFC signals were in close apposition to the TGN46 signal, confirming that the SCAP–Sac1 and SCAP–VAP-A interactions occur at ER–Golgi MCSs (Fig. 3, E and F).

To further substantiate that the perinuclear Vn-SCAP–Vc-Sac1 and Vn-SCAP–Vc-VAP-A BiFC signals represent the interaction of SCAP in the ER but not in the Golgi complex, we examined the effect of cholesterol depletion. As reported previously (Nohturfft et al., 2000), cholesterol depletion using lipoprotein-deficient serum and 2-hydroxypropyl-β-cyclodextrin caused redistribution of a part of the SCAP pool from the ER to the cis/medial-Golgi membranes (Fig. S3, A and B) accompanied by SREBP2 cleavage (Fig. S3 C). In contrast to 25-HC treatment, cholesterol depletion did not enhance either the Vn-SCAP–Vc-Sac1 or Vn-SCAP–Vc-VAP-A interaction (Fig. 3, A and B, bottom rows; and Fig. 3, C and D). Altogether, these results suggest that ER-localized SCAP preferentially interacts with VAP-A, OSBP, and Sac1 at ER–Golgi MCSs.

SCAP is important for PI4P turnover and VAP-A–OSBP complex distribution at ER–Golgi MCSs

The finding that SCAP forms a complex with VAP-A, OSBP, and Sac1 at ER–Golgi MCSs prompted us to examine whether SCAP is involved in the counter-transport of ER cholesterol and Golgi PI4P at ER–Golgi MCSs. To address this issue, we performed knockdown of SCAP in HeLa cells. By using siRNA, the expression of SCAP was decreased to ∼16% of the control level (Fig. 4 A). In response to cholesterol deprivation, the SCAP–SREBP pathway stimulates transcription of genes responsible for cholesterol synthesis and uptake, such as *3-hydroxy-3-methylglutaryl coenzyme A reductase* (*HMGR*) and *low-density lipoprotein receptor* (*LDLR*; Brown and Goldstein, 1997; Horton et al., 2003). However, under cholesterol-fed conditions (that is, culturing of cells in normal medium supplemented with FCS as a source of sterols), SCAP knockdown did not reduce the transcription of either *HMGR* or *LDLR* genes, but rather slightly increased *LDLR* mRNA levels (Fig. 4 B). Consistently, no significant change in total cholesterol level was observed upon SCAP knockdown (Fig. 4 C). Similar results were obtained for HeLa cells stably expressing shRNA targeting SCAP (shSCAP cells) with reduced expression of SCAP (∼8% of that in parental HeLa cells), but not of HMGR and LDLR (Fig. 4, D–F).

Staining of parental HeLa and shSCAP cells with the fluorescent cholesterol probe filipin showed no significant difference

Downloaded from http://rupress.org/jcb/article-pdf/220/1/e202002150/1617891/jcb_202002150.pdf by guest on 06 May 2026

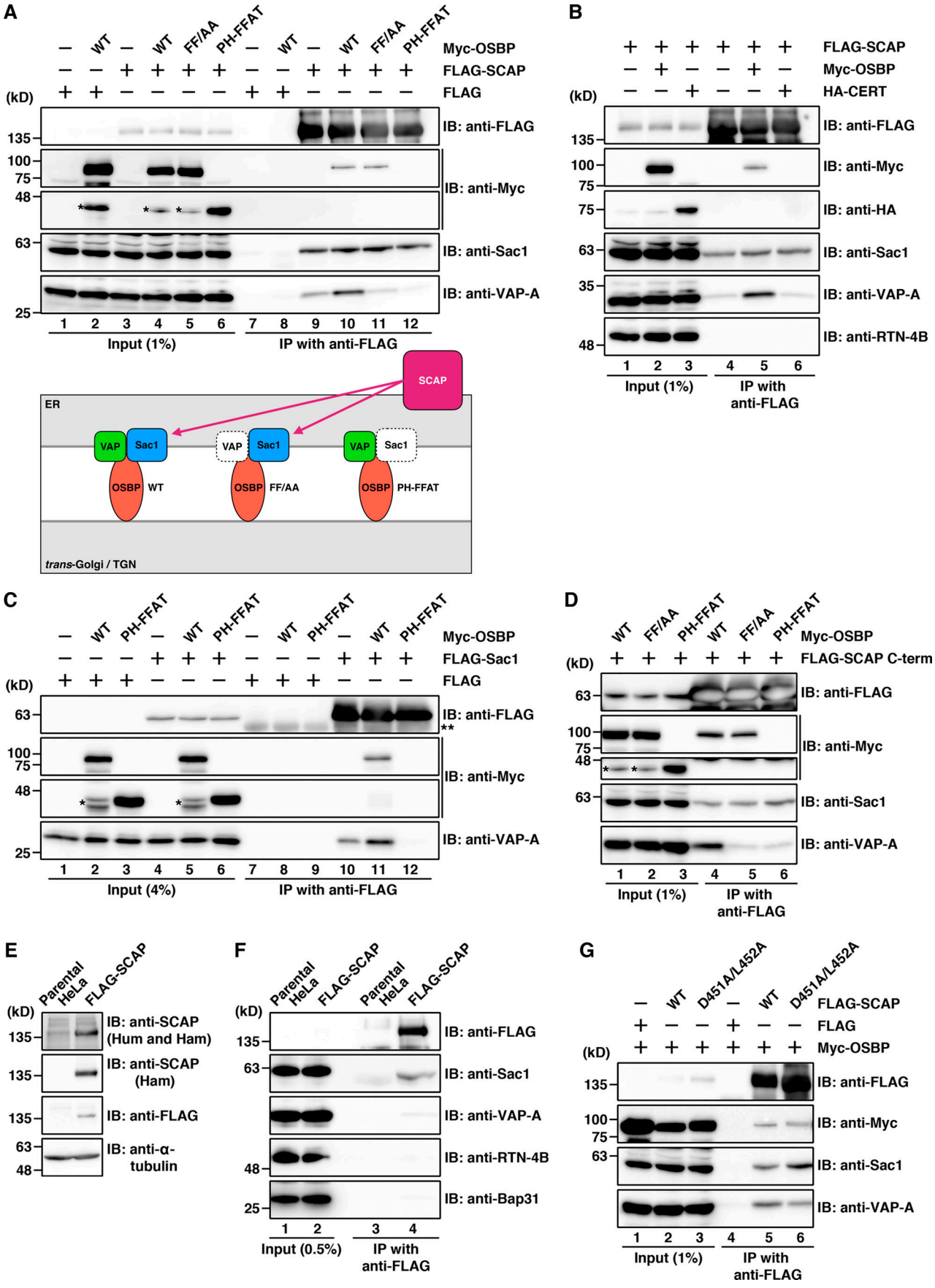

Downloaded from http://rupress.org/jcb/article-pdf/220/1/e202002150/1617891/jcb_202002150.pdf by guest on 06 May 2026

Figure 2. **ER-localized SCAP interacts through Sac1 with the VAP-A–OSBP complex. (A)** Interactions of FLAG-SCAP with Myc-OSBP, Sac1, and VAP-A in HEK 293T cells. Bottom panel shows a schematic representation of the SCAP interactions with VAP, OSBP, and Sac1. **(B)** Interactions of FLAG-SCAP with Myc-OSBP, Sac1, and VAP-A, but not with HA-CERT or RTN-4B. **(C)** Interactions of FLAG-Sac1 with VAP-A and Myc-OSBP WT, but not with the PH-FFAT mutant. **(D)** Interactions of FLAG-SCAP C-term with Myc-OSBP, Sac1, and VAP-A. **(E)** Establishment of a HeLa stable cell line expressing FLAG-SCAP. Ham, hamster; Hum, human. **(F)** Interaction of stably expressed FLAG-SCAP with Sac1, but not with RTN-4B or Bap31. VAP-A was detected as a very faint band in the immunoprecipitate (IP) of the stable cell line (lane 4). **(G)** Interactions of the FLAG-SCAP D451A/L452A mutant with Myc-OSBP, Sac1, and VAP-A. Single and double asterisks denote degraded Myc-OSBP fragments and the Ig heavy chain, respectively. IB, immunoblotted.

in the intracellular distribution of cholesterol between these cell lines (Fig. 5 A). Although a part of the perinuclear signal of filipin overlapped with that of a TGN marker, Golgin-97, most of the signal was thought to be derived from other membranous structures, as shown previously (Ikonen, 2018), and filipin does not seem to have sufficient sensitivity to detect low levels of cholesterol in the ER and Golgi membranes.

Because of the lack of cholesterol probes with enough sensitivity for our purposes, we focused on monitoring the PI4P level in SCAP knockdown cells. When PI4P was visualized with a specific antibody, the fluorescence signal in shSCAP cells was significantly increased compared with that in the parental HeLa cells, especially in the juxtanuclear region that partially overlapped with membranes positive for the TGN markers sialyltransferase and Golgin-97 (Fig. 5, B and C). Similar phenotypes were observed in VAP-A/B or CERT/OSBP double-knockdown cells, as well as in Sac1 knockdown cells (Fig. S4 A). Taken together, our data suggest that SCAP regulates the TGN PI4P levels by controlling the turnover of PI4P at ER–Golgi MCSs.

Next, we evaluated the effect of SCAP knockdown on the formation of the VAP-A–OSBP complex by using the BiFC approach. A stable cell line coexpressing Vn-OSBP and Vc-VAP-A showed a BiFC signal in the juxtanuclear region, which was enhanced by 25-HC treatment (Fig. S4 B). When SCAP was knocked down by siRNA, ∼34% of cells showed a bright BiFC signal in the peripheral region in addition to the signal at the juxtanuclear Golgi region, and the number of cells with this phenotype increased to ∼61% upon 25-HC treatment (Fig. 5 D).

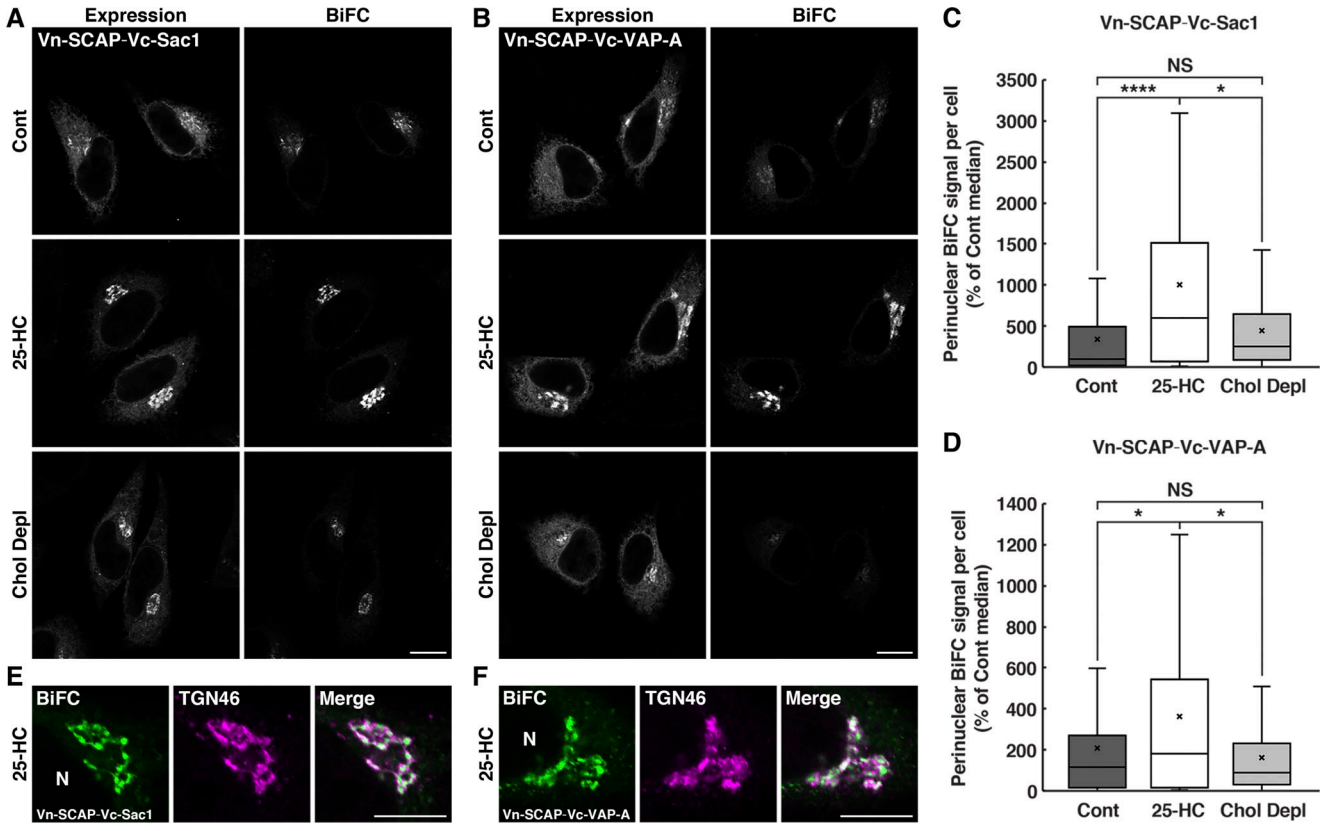

Figure 3. **BiFC visualization of SCAP, VAP-A, and Sac1 interactions at ER–Golgi MCSs. (A–F)** BiFC visualization of the SCAP–Sac1 or SCAP–VAP-A interaction at ER–Golgi MCSs in HeLa cells coexpressing Myc-OSBP and Vn-fused SCAP in combination with Vc-fused Sac1 (A, C, and E) or VAP-A (B, D, and F). The cells were incubated without (Control [Cont]) or with 2 µg/ml 25-HC for 2.5 h or were cholesterol depleted (Chol Depl) for 3 h. The expression of Vn-SCAP together with Vc-Sac1 (A) or Vc-VAP-A (B) was visualized with an anti-GFP antibody. **(C and D)** Quantification of perinuclear BiFC signal. Boxes delimit the first and third quartiles and the central line is the median, whereas the cross represents the mean value. The whiskers represent the minimum and maximum values after outlier removal (n = 70–101 cells per condition; *, $P < 0.05$; ****, $P < 0.0001$; Kruskal-Wallis multiple sample nonparametric test). N, nucleus. Scale bars, 10 µm.

Downloaded from http://rupress.org/jcb/article-pdf/220/1/e202002150/1617891/jcb_202002150.pdf by guest on 06 May 2026

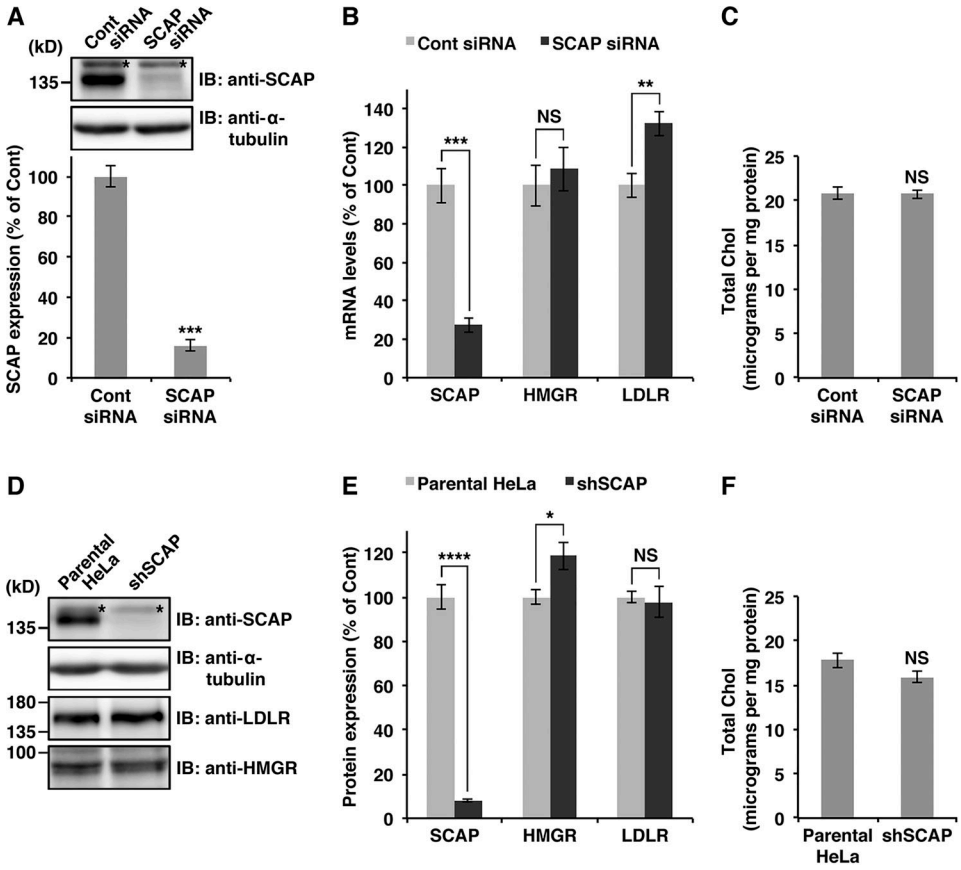

Figure 4. **SCAP knockdown does not disrupt cholesterol metabolism under cholesterol-fed conditions. (A)** siRNA-mediated knockdown of SCAP in HeLa cells. The graph shows determination of the expression levels of SCAP at 72 h after siRNA transfection. Data are means ± SEM (n = 3 independent experiments; ***, P < 0.001; unpaired two-tailed Student's t test). **(B)** Determination of mRNA levels of the indicated genes in control (Cont) and SCAP knockdown cells by quantitative real-time PCR. Data are means ± SEM (n = 4 independent experiments; **, P < 0.01; ***, P < 0.005; unpaired two-tailed Student's t test). **(C)** Total cholesterol (Chol) levels in control and SCAP knockdown cells. Data are means ± SEM (n = 6 independent experiments; unpaired two-tailed Student's t test). **(D and E)** shRNA-mediated knockdown of SCAP in HeLa cells. **(E)** Expression levels of SCAP, HMGR, and LDLR in parental HeLa (control) and shSCAP HeLa cells. Data are means ± SEM (n = 4 independent experiments; *, P < 0.05; ****, P < 0.001; unpaired two-tailed Student's t test). **(F)** Total cholesterol levels in parental HeLa and shSCAP HeLa cells. Data are means ± SEM (n = 3 independent experiments; unpaired two-tailed Student's t test). Asterisks on the Western blots denote nonspecific bands. IB, immunoblotted.

As the VAP–OSBP complex has been reported to exist not only at ER–Golgi MCSs but also at ER–endosome MCSs (Dong et al., 2016), we compared the localization of the peripheral BiFC signal with that of the late endosomal marker CD63. The close apposition of CD63 but not of TGN46 to the peripheral BiFC signal was observed in SCAP knockdown cells (Fig. 5 E), indicating that SCAP is required to prevent the redistribution of the VAP-A–OSBP complex to ER–endosome MCSs and to maintain it at ER–Golgi MCSs.

SCAP is required for the biogenesis of CARTS at the TGN

We previously reported that perturbation of lipid transfer complexes at ER–Golgi MCSs inhibits the biogenesis of CARTS at the TGN (Wakana et al., 2015). Here, we visualized CARTS in Vn-OSBP–Vc-VAP-A stably expressing cells treated with 25-HC by staining a CARTS-specific cargo, pancreatic adenocarcinoma up-regulated factor (PAUF; Wakana et al., 2012). Putative nascent CARTS imaged by super-resolution stimulated emission depletion (STED) microscopy were located in the close vicinity of the BiFC-positive perinuclear structures (Fig. 6 A, arrowheads), suggesting that CARTS form at sites immediately adjacent to the VAP-A–OSBP complex-containing ER–Golgi MCSs. Next, we investigated whether SCAP is required for CARTS-mediated protein secretion. In SCAP knockdown cells, the secretion of PAUF-MycHis was reduced to ∼49% of that in control cells (Fig. 6 B). Moreover, PAUF-MycHis secreted by SCAP knockdown cells was detected as a smeared band, suggesting a defect in PAUF processing, as previously observed in cells depleted of other ER–Golgi contact site components (Wakana et al., 2015).

The effect of SCAP knockdown on the biogenesis of CARTS was assessed with an inducible CARTS formation assay, where synchronized transport of PAUF from the ER was performed by using a reverse dimerization system involving D/D solubilizer-induced disassembly of FM4 domains (Rivera et al., 2000). The chimera protein mKate2-FM4-PAUF initially retained in the ER lumen was first exported from this organelle and accumulated in the Golgi membranes by D/D solubilizer treatment at 20°C for 45 min, after which the temperature was shifted to 37°C to induce the formation of mKate2-FM4-PAUF–containing CARTS at the TGN. Live-cell imaging showed that a large number of

Downloaded from http://rupress.org/jcb/article-pdf/220/1/e202002150/1617891/jcb_202002150.pdf by guest on 06 May 2026

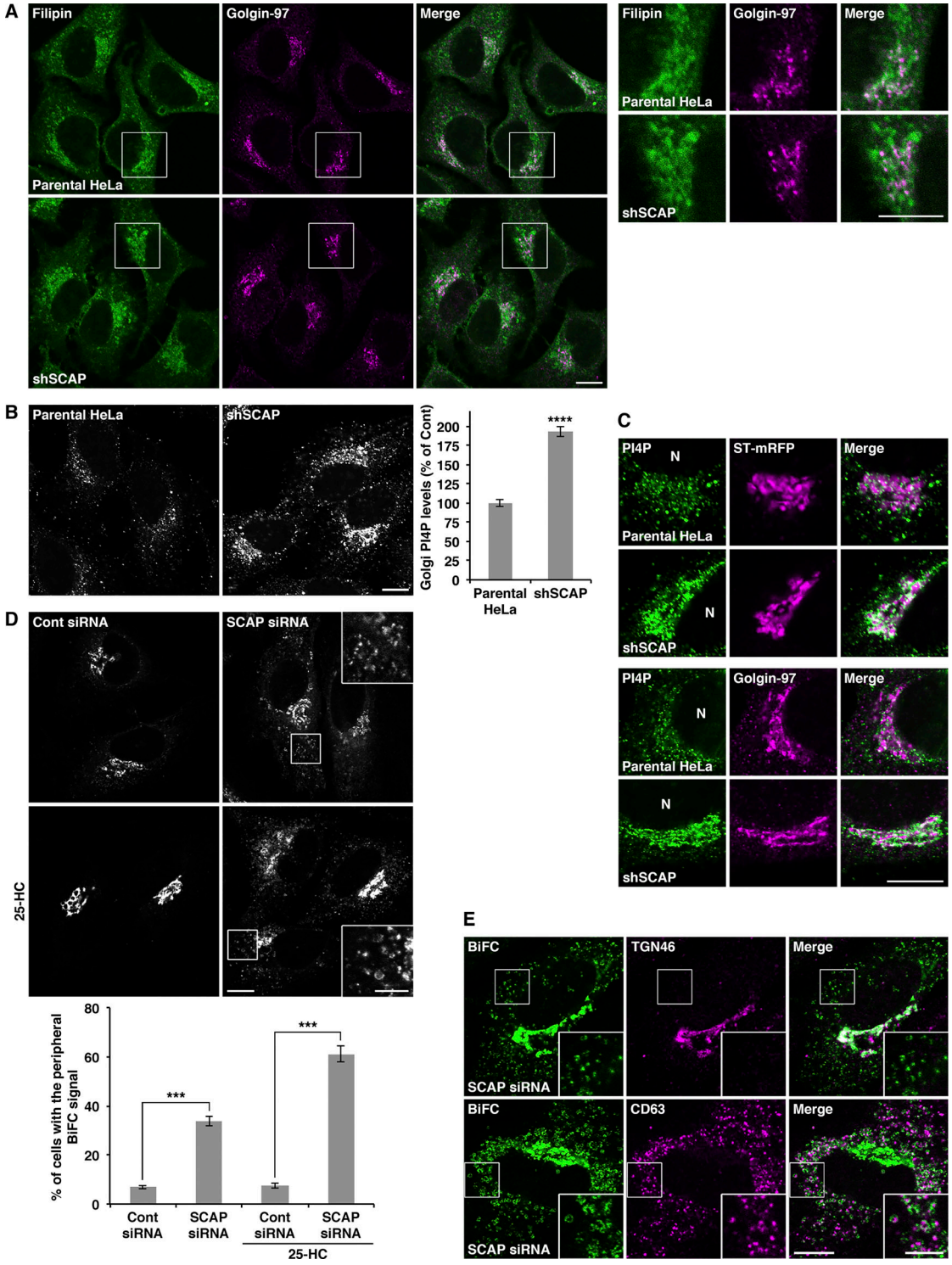

Figure 5. **SCAP is important for PI4P turnover and VAP-A–OSBP complex distribution at ER–Golgi MCSs. (A)** Filipin staining in parental HeLa and shSCAP HeLa cells. High magnifications of the boxed areas are shown in the right panels. **(B and C)** PI4P staining in parental HeLa and shSCAP HeLa cells with (top two rows in C) or without (B and bottom two rows in C) sialyltransferase (ST)–mRFP expression. The graph shows determination of the Golgi PI4P levels in parental HeLa (control) and shSCAP HeLa cells. Data are means ± SEM (n = 139 cells per condition; ****, P < 0.0001; unpaired two-tailed Student's t test). N, nucleus. **(D)** BiFC visualization of the OSBP–VAP-A interaction in control (Cont) and SCAP knockdown cells. HeLa cells stably coexpressing Vn-OSBP and Vc-VAP-A were transfected with siRNA. After 72 h, the cells were treated with or without 2 µg/ml 25-HC for 2.5 h. High magnifications of the boxed areas are shown in the insets where brightness/contrast enhancement was applied. The graph shows the percentage of cells with the peripheral BiFC signal of Vn-OSBP–Vc-VAP-A. Data are means ± SEM (n = 3 independent experiments; 100–131 cells per condition; ***, P < 0.005; unpaired two-tailed Student's t test). **(E)** Close apposition of CD63- but not of TGN46-positive membranes to the peripheral BiFC signal of Vn-OSBP–Vc-VAP-A in SCAP knockdown cells treated with 2 µg/ml 25-HC for 2.5 h. High magnifications of the boxed areas are shown in the insets. Scale bars, 10 µm (large panels), 5 µm (insets).

Downloaded from http://rupress.org/jcb/article-pdf/220/1/e202002150/1617891/jcb_202002150.pdf by guest on 06 May 2026

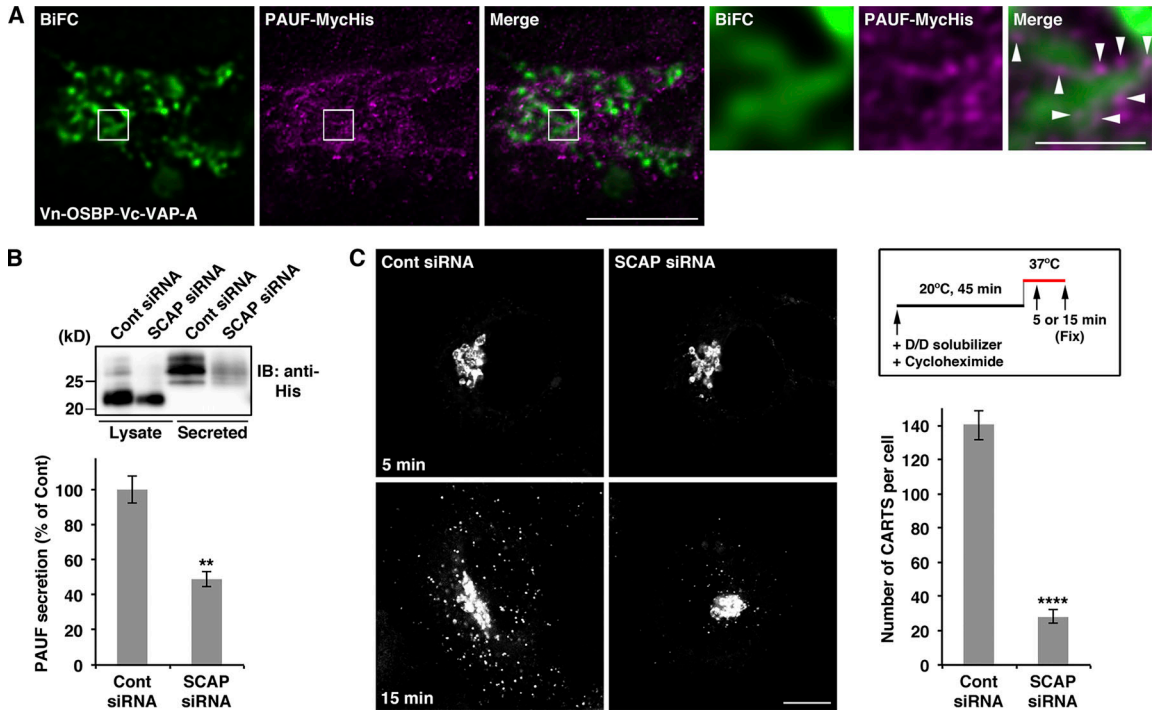

Figure 6. **SCAP is required for the biogenesis of CARTS at the TGN. (A)** Close proximity of CARTS formation sites (PAUF-MycHis channel, imaged by STED) to VAP-A–OSBP–mediated ER–Golgi MCSs (BiFC channel, imaged by confocal microscopy). Images were acquired and deconvolved as described in Materials and methods. High magnifications of the boxed areas are shown in the right panels. Arrowheads indicate putative nascent CARTS located in the close vicinity of the BiFC signal of Vn-OSBP–Vc-VAP-A. Scale bars, 5 µm (left panels), 1 µm (right panels). **(B)** PAUF-MycHis secretion in control (Cont) and SCAP knockdown cells. The graph shows quantification of secreted PAUF-MycHis relative to the total cellular level and normalized as the values in control cells. Data are means ± SEM (n = 3 independent experiments; **, P < 0.01; unpaired two-tailed Student's t test). IB, immunoblotted. **(C)** Biogenesis of mKate2-FM4-PAUF–containing CARTS in control and SCAP knockdown cells. The graph shows the number of mKate2-FM4-PAUF–containing CARTS in control and SCAP knockdown cells at 15 min after the temperature shift to 37°C. Data are means ± SEM (n = 20–29 cells per condition; ****, P < 0.0001; unpaired two-tailed Student's t test). Scale bar, 10 µm. See also Video 1.

CARTS were formed at the TGN membranes and dispersed throughout the cytoplasm (Video 1). Next, mKate2-FM4-PAUF was expressed in control and SCAP knockdown cells. At 15 min after the temperature shift to 37°C, the average number of CARTS in SCAP knockdown cells was ∼20% of that in control cells (Fig. 6 C).

In our model, lipid transfer at ER–Golgi MCSs is thought to promote CARTS biogenesis through organization of cholesterol- and SM-enriched nanodomains at the TGN (Wakana et al., 2015). We therefore examined the effect of SCAP knockdown on transport of glycosylphosphatidyl inositol (GPI)–anchored protein, which has been reported to associate with cholesterol- and sphingolipid-enriched detergent-insoluble membranes (Brown and Rose, 1992; Simons and Ikonen, 1997; Mayor and Riezman, 2004; Deng et al., 2016). Synchronized transport of mKate2-FM4-GPI from the ER to the PM was initiated by the addition of D/D solubilizer, as previously reported (Deng et al., 2016). As shown in Fig. 7 A, SCAP knockdown did not affect transport of mKate2-FM4-GPI from the ER (0 min) to the Golgi complex (30 min). Nevertheless, at 60 min after transport initiation, the amount of mKate2-FM4-GPI that had reached the cell surface was significantly decreased in SCAP knockdown cells. At 90 min, most of the protein had been transported to the PM in control cells, but in ∼41% of SCAP knockdown cells, the protein was still localized to the TGN (Fig. 7, A and B). Similar results were obtained with knockdown of VAP-A/B, CERT/OSBP, or, to a lesser extent, OSBP (Fig. 7 A and Fig. S5 A). In addition to these results, overexpression of OSBP PH-FFAT, which immobilizes ER–Golgi MCSs and inhibits CARTS biogenesis (Wakana et al., 2015), strongly inhibited mKate2-FM4-GPI export from the TGN (Fig. S5 B). We also tested transport of vesicular stomatitis virus G protein (VSV-G), which is exported from the TGN in carriers distinct from CARTS (Wakana et al., 2012, 2013). SCAP knockdown did not significantly delay TGN-to-PM transport of VSV-G–GFP (Fig. S5 C) compared with that of mKate2-FM4-GPI (Fig. 7 A).

Next, we tested if CARTS are the carriers that transport mKate2-FM4-GPI from the TGN to the cell surface. When mKate2-FM4-GPI and PAUF-MycHis were coexpressed in cells, we observed that mKate2-FM4-GPI was included in PAUF-MycHis–positive CARTS, although its fluorescence signal was relatively low (Fig. 7 C). Consistent with our previous finding that CARTS biogenesis requires PKD-mediated membrane fission at the TGN (Wakana et al., 2012), export of mKate2-FM4-GPI from the TGN was inhibited by expression of a dominant-negative kinase-dead (KD) mutant of PKD2. Even at 90 min after transport initiation, the protein was included in TGN-derived tubules, most likely corresponding to fission-defective precursors of

Downloaded from http://rupress.org/jcb/article-pdf/220/1/e202002150/1617891/jcb_202002150.pdf by guest on 06 May 2026

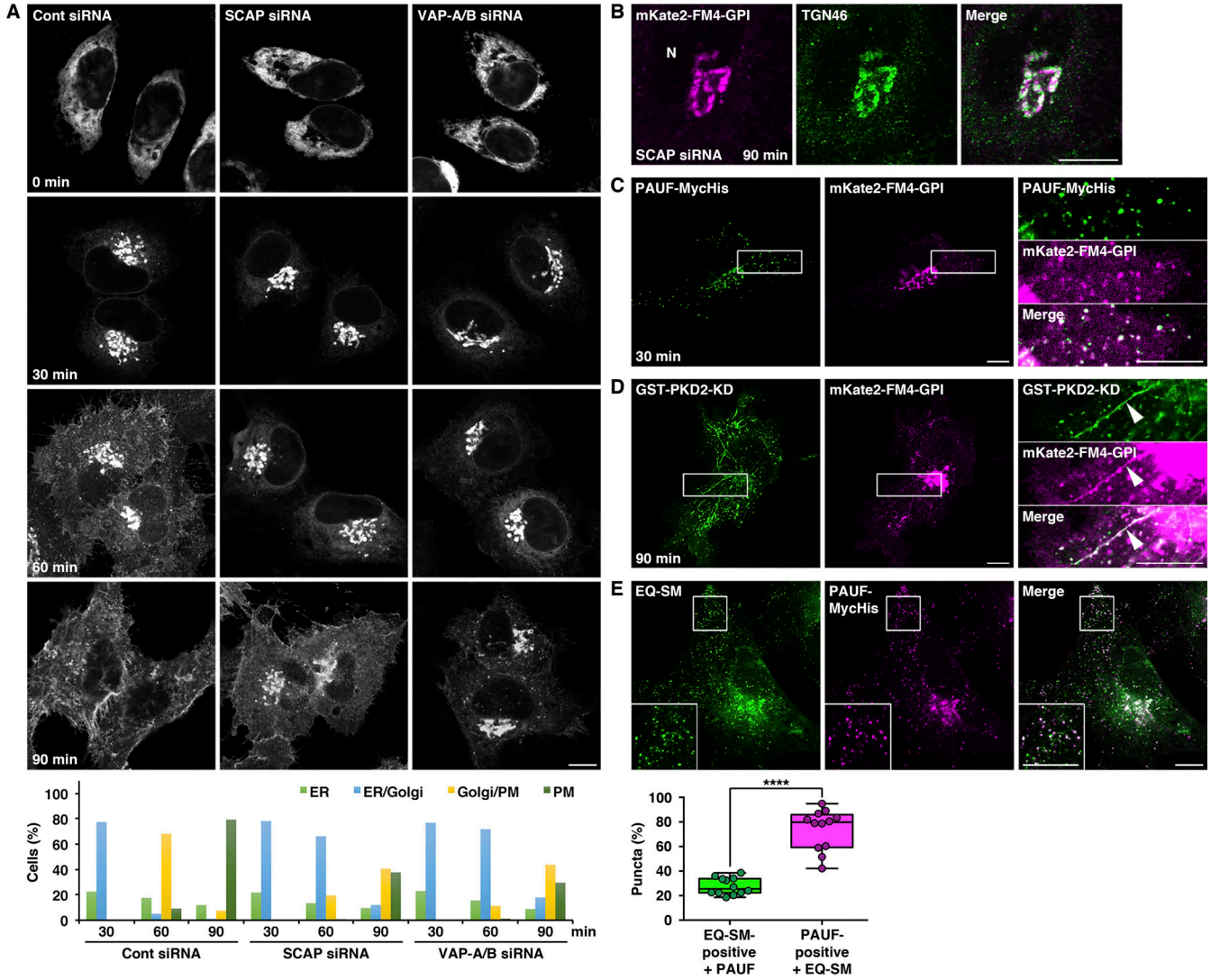

Figure 7. **SCAP is required for GPI-anchored protein transport from the TGN to the PM. (A)** mKate2-FM4-GPI transport from the ER to the PM via the Golgi complex in control (Cont), SCAP, and VAP-A/B knockdown cells. The graph shows the percentages of cells with mKate2-FM4-GPI at the ER, ER/Golgi, Golgi/PM, or PM at the indicated times. The data shown are for a single representative experiment out of three performed (n = 230–252 cells per condition). **(B)** mKate2-FM4-GPI has accumulated at the TGN at 90 min after the transport induction in SCAP knockdown cells. N, nucleus. **(C)** Colocalization of PAUF-MycHis and mKate2-FM4-GPI in CARTS at 30 min after the transport induction. **(D)** Colocalization of GST-PKD2-KD and mKate2-FM4-GPI in tubules attached to the TGN at 90 min after the transport induction. **(C and D)** High magnifications of the boxed areas are shown in the right column where brightness/contrast enhancement was applied to the mKate2-FM4-GPI channel. Arrowheads in D indicate a GST-PKD2-KD–induced tubule containing mKate2-FM4-GPI. **(E)** Colocalization of EQ-SM and PAUF-MycHis. High magnifications of the boxed areas are shown in the insets. The box-and-whisker plots show quantification of EQ-SM–positive puncta containing PAUF-MycHis (green) and PAUF-MycHis–positive puncta containing EQ-SM (magenta). Boxes delimit the first and third quartiles, and the central line is the median. The whiskers represent the minimum and maximum values after outlier removal (EQ-SM positive: n = 4,487 puncta; PAUF positive: n = 1,650 puncta in 12 cells; ****, $P < 0.0001$; paired two-tailed Student's t test). Scale bars, 10 µm.

transport carriers, such as CARTS (Fig. 7 D, arrowheads). Previous work revealed that a nontoxic SM reporter protein, EQ-SM, is enriched in transport carries containing mKate2-FM4-GPI (Deng et al., 2016). When EQ-SM and PAUF-MycHis were coexpressed in cells, ∼80% of PAUF-MycHis–positive CARTS contained EQ-SM (Fig. 7 E). This result fits well with the former report that 86 ±5% of mKate2-FM4-GPI–positive exocytic vesicles contain EQ-SM (Deng et al., 2016).

Taken together, these results strongly suggest that SCAP specifically promotes the biogenesis of CARTS, which are enriched in cholesterol and SM.

SCAP regulates CARTS biogenesis in a cholesterol-dependent manner

SCAP directly binds cholesterol and plays a pivotal role in cholesterol homeostasis as a cholesterol sensor in the ER membrane (Radhakrishnan et al., 2004; Motamed et al., 2011; Brown et al., 2018). Does SCAP regulate CARTS biogenesis by sensing the ER cholesterol level? Previous mutagenesis analysis of SCAP in CHO cells revealed that several amino acid residues are critical for the conformational change induced by cholesterol binding (Brown et al., 2018). Specifically, replacement of tyrosine 234 in the cholesterol-binding loop 1 region of SCAP (Fig. 8 A) with alanine

Downloaded from http://rupress.org/jcb/article-pdf/220/1/e202002150/1617891/jcb_202002150.pdf by guest on 06 May 2026

(Y234A) abolishes binding of loop 1 to loop 7, and thus, this mutant binds to Insig even in the absence of cholesterol (Motamed et al., 2011). By contrast, mutants with replacement of tyrosine 298, leucine 315, and aspartic acid 443 in the sterol-sensing domain (SSD; Fig. 8 A, highlighted in light blue) with cysteine (Y298C), phenylalanine (L315F), and asparagine (D443N), respectively, are resistant to the cholesterol-induced conformational change and show no Insig binding, even in the presence of sterols (Nohturfft et al., 1998; Brown et al., 2002; Yabe et al., 2002a, b; Yang et al., 2002; Adams et al., 2003).

We established different shSCAP cells, each of which stably expressed hamster SCAP WT, Y234A, Y298C, L315F, D443N, or D451A/L452A (Golgi transport–defective mutant). Western blotting of cell lysates with an antibody specific to hamster SCAP and one recognizing both hamster and human SCAP showed higher expression levels of exogenous proteins, except for D443N, than those of endogenous SCAP in parental HeLa cells (Fig. 8 B). Immunofluorescent staining with an anti-hamster SCAP antibody showed reticular distributions of WT, Y234A, Y298C, and D451A/L452A in the ER and additional Golgi-localized pools of L315F and D443N under cholesterol-fed conditions (Fig. S3 D, first and third rows). A previous work reported that SCAP Y298C is redistributed to the Golgi complex even in the presence of sterols, based on data obtained with digestion of N-linked carbohydrates of SCAP by endoglycosidase H (Nohturfft et al., 1998). However, at the level of immunofluorescence microscopy, the signal of Y298C in the Golgi complex was not obvious, because most of the protein was present in the juxtanuclear ER (Fig. S3 D, upper right panel). Perhaps, a minor fraction of the Y298C pool is transported to the Golgi complex and acquires endoglycosidase H resistance. When cholesterol was depleted from cells, fractions of the WT and Y298C pools were redistributed from the ER to the Golgi complex, whereas Y234A and D451A/L452A remained in the ER (Fig. S3 D, second and fourth rows), in agreement with previous reports (Nohturfft et al., 1998; Yabe et al., 2002a; Motamed et al., 2011). Since only a small number of cells expressed D443N, this cell line was not used in subsequent experiments.

We examined the effect that the expression of the respective hamster SCAP proteins has on the turnover of PI4P and CARTS biogenesis. Our results showed that expression of WT, but not Y234A, Y298C, or L315F, reversed the accumulation of PI4P at the TGN (Fig. 8 C). Consistently, expression of SCAP WT caused the recovery of the number of CARTS from SCAP knockdown, but neither Y234A, Y298C, nor L315F showed such an effect (Fig. 8 D). It is of note that expression of the Golgi transport–defective mutant D451A/L452A recovered both functions, similarly to WT (Fig. 8, C and D). These results suggest that the cholesterol-sensing ability of SCAP in the ER membrane is required for CARTS biogenesis and is tightly linked to the capacity of SCAP to regulate PI4P turnover at ER–Golgi MCSs.

The SCAP–SREBP complex functions in CARTS biogenesis

SCAP and SREBPs are known to form a stable complex. Consistent with previous reports (Rawson et al., 1999; Matsuda et al., 2001; Moon et al., 2012), expression levels of SREBP1 and SREBP2 were also significantly decreased in shSCAP cells (Fig. 9 A, lane 2). Importantly, while expression of not only SCAP WT or D451A/L452A but also Y234A, Y298C, or L315F recovered expression of SREBPs (Fig. 9 A, lanes 3–7), these cholesterol-sensing defective mutants were not able to rescue the defects in PI4P turnover and CARTS biogenesis (Fig. 8, C and D). These results suggest that the cholesterol-sensing ability of SCAP, and not the presence of SREBPs, is the dominant factor by which SCAP controls these functions. Immunoprecipitation of FLAG-SREBP1a and FLAG-SREBP2 showed their interactions with Myc-OSBP and endogenous Sac1 and VAP-A (Fig. 9 B). Our observation that FLAG-SREBPs show a higher affinity for GFP-SCAP than for components of the cholesterol/PI4P exchange machinery (Fig. 9 C) suggests that SCAP and SREBPs form a stable complex that only transiently interacts with the lipid exchange machinery at ER–Golgi MCSs.

Finally, we tested whether knockdown of SREBPs affects CARTS biogenesis. The expression levels of SREBP1 and SREBP2 were significantly decreased by using siRNA targeting a common sequence of two alternative splicing isoforms of SREBP1 (1a and 1c) and SREBP2, respectively, without affecting expression of SCAP (Fig. 9 D, lanes 1–3). Since a mixture of these two siRNAs did not reduce SREBP1 and SREBP2 at the same time (Fig. 9 D, lane 4), the effect on CARTS formation of either SREBP1 or SREBP2 knockdown was examined. Our results showed that the average number of CARTS was decreased to ∼74% and 39% of the control levels in SREBP1 and SREBP2 knockdown cells, respectively (Fig. 9 E).

Discussion

SCAP was discovered in 1996 as an ER protein whose mutation conferred on CHO cells resistance to 25-HC, an oxygenated cholesterol derivative that suppresses SREBP processing and thereby blocks cholesterol synthesis but cannot replace cholesterol for cell viability (Hua et al., 1996). Subsequent studies demonstrated that SCAP senses the ER cholesterol content and, in response to cholesterol deficiency, escorts SREBPs from the ER to the Golgi complex for their cleavage-mediated activation (Brown et al., 2018).

In the present study, we demonstrate a new function of SCAP under cholesterol-fed conditions. Based on our data, we propose a model whereby SCAP interacts with VAP–OSBP at ER–Golgi MCSs via Sac1 and regulates counter-transport of cholesterol and PI4P in an ER cholesterol–dependent manner (Fig. 10). This is supported by our finding that SCAP knockdown causes accumulation of PI4P at the TGN (Fig. 5, B and C), a hallmark of the impairment of cholesterol/PI4P exchange between the ER and the trans-Golgi membranes. SCAP appears to contribute to the efficient establishment of ER–Golgi MCSs because its knockdown caused partial redistribution of the VAP–OSBP complex to ER–endosome MCSs (Fig. 5, D and E). At the trans-Golgi membranes, cholesterol and SM organize lipid nanodomains, which can function as a platform for molecular machineries responsible for processing and sorting of cargoes, including GPI-anchored proteins (Fig. 10, right panel). In parallel, DAG, which is synthesized together with SM from ceramide and phosphatidylcholine, recruits PKD for membrane fission, leading to

Downloaded from http://rupress.org/jcb/article-pdf/220/1/e202002150/1617891/jcb_202002150.pdf by guest on 06 May 2026

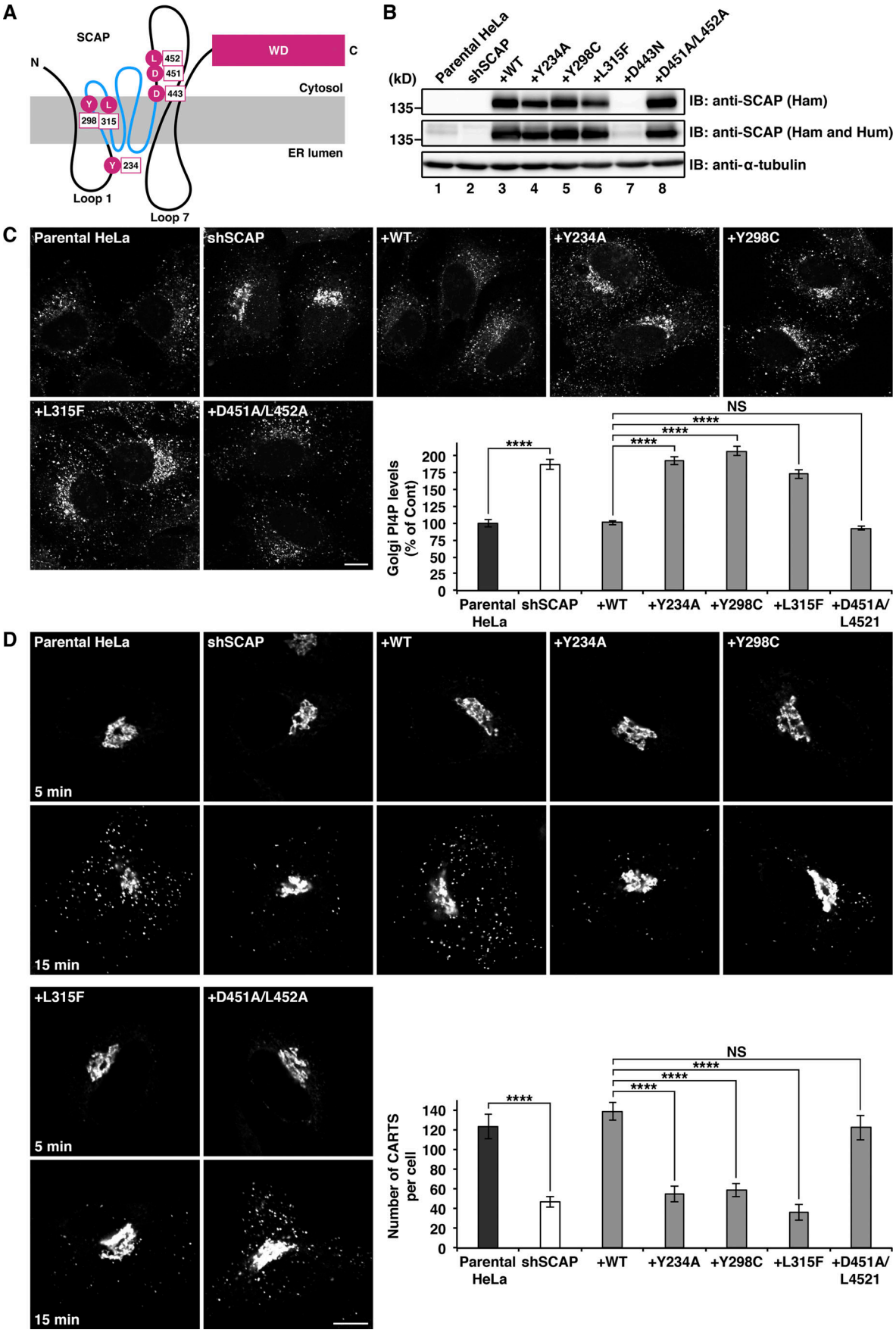

Downloaded from http://rupress.org/jcb/article-pdf/220/1/e202002150/1617891/jcb_202002150.pdf by guest on 06 May 2026

Figure 8. **SCAP regulates CARTS biogenesis in a cholesterol-dependent manner. (A)** Schematic representation of the SCAP topology. SSD is highlighted in light blue. N, N-terminus; C, C-terminus. **(B)** Establishment of shSCAP HeLa cells stably expressing the hamster SCAP WT and mutants. IB, immunoblotted. **(C)** Recovery of PI4P turnover on expression of hamster SCAP WT or D451A/L452A, but not of Y234A, Y298C, or L315F. The graph shows determination of the Golgi PI4P levels in the indicated cells. Data are means ± SEM (n = 69–96 cells per condition; ****, P < 0.0001; one-way ANOVA multiple comparison test). **(D)** Recovery of the biogenesis of mKate2-FM4-PAUF–containing CARTS on expression of hamster SCAP WT or D451A/L452A, but not of Y234A, Y298C, or L315F. The graph shows the number of mKate2-FM4-PAUF–containing CARTS in the indicated cells at 15 min after the temperature shift to 37°C. Data are means ± SEM (n = 20 cells per condition; ****, P < 0.0001; one-way ANOVA multiple comparison test). Scale bars, 10 µm.

CARTS biogenesis. Intriguingly, our finding of putative nascent CARTS in the close vicinity of ER–Golgi MCSs (Fig. 6 A) suggests a possible role for the ER contacts in determining the position for membrane fission, analogous to their important role in mitochondrial and endosomal fission (Friedman et al., 2011; Rowland et al., 2014).

Cytoplasmic coats generally provide a means to coordinate signal-mediated cargo sorting with carrier budding and membrane fission. However, most TGN-derived transport carriers, including CARTS, lack cytoplasmic coats, and therefore, such molecular mechanisms remain largely elusive for these transport carriers (Wakana et al., 2012; Pakdel and von Blume, 2018). A recent paper reported that Ca^{2+}-dependent and oligomerization-driven cargo sorting, which is mediated by the SPCA1 Ca^{2+} pump and the secreted Ca^{2+}-binding protein Cab45, is coupled to local SM synthesis at the TGN (Deng et al., 2018). The finding that sorting of lysozyme C, one of the secretory cargoes in CARTS (Wakana et al., 2012), is controlled by this mechanism strongly supports our model.

Our data showed that neither the loop 1 nor the SSD mutants, which reflect different conformations in the context of Insig binding, are competent for PI4P turnover and CARTS biogenesis (Fig. 8, C and D). These findings imply that conformational switching that reflects cholesterol-free and -bound states is important. Considering that the ER contains low levels of cholesterol, it is tempting to speculate that SCAP functions as a cholesterol recruiter in the ER membrane to present it to cytosolic OSBP for efficient cholesterol transfer at ER–Golgi MCSs, which may explain why the two different types of mutants revealed similar phenotypes. It is worth mentioning that SCAP knockdown dramatically altered the distribution of the VAP–OSBP complex in the presence of 25-HC (Fig. 5 D). As 25-HC directly binds to OSBP (Ridgway et al., 1992; Suchanek et al., 2007) but indirectly to SCAP via Insig (Adams et al., 2004; Radhakrishnan et al., 2007), this finding reveals the possibility that SCAP functions at ER–Golgi MCSs as a complex with Insig as well as SREBPs, supported by a previous finding that Insig interacts with VAP-A and VAP-B (Gong et al., 2006).

In conclusion, our findings reveal a new role of SCAP under cholesterol-fed conditions and provide insights into the regulatory mechanisms for lipid transfer at ER–Golgi MCSs for transport carrier biogenesis at the TGN.

Materials and methods

Antibodies and reagents

Monoclonal antibodies were procured as follows: FLAG (F3165, clone M2) and α-tubulin (T6074, clone B-5-1-2) were purchased from Sigma-Aldrich; Myc (sc-40, clone 9E10), hamster SCAP (sc-13553, clone 9D5), and HMGR (sc-271595, clone C-1) from Santa Cruz Biotechnology; SREBP1 (04–469, clone 2121) from EMD Millipore; Penta-His (34660) from Qiagen; CD63 (clone H5C6) from the Developmental Studies Hybridoma Bank; calnexin (610524, clone 37) and GM130 (610823, clone 35) from BD Biosciences; and PI4P (Z-P004) from Echelon Biosciences. Polyclonal antibodies were procured as follows: HA (sc-805), Nogo (RTN-4B; sc-11027), SCAP (sc-9675), and GST (sc-459) from Santa Cruz Biotechnology; SCAP (A303-554A) from Bethyl Laboratories; SACM1L (Sac1; 13033-1-AP) from Proteintech; TGN46 (AHP500GT) from AbD Serotec; GFP (A6455) from Thermo Fisher Scientific; SREBP2 (ab30682), LDLR (ab52818), and Golgin-97 (ab84340) from Abcam; GPP130 (923801) from BioLegend; and Myc (2272) from Cell Signaling Technology. Control rabbit IgG (011–000-003) was purchased from Jackson ImmunoResearch. To raise rabbit polyclonal antibodies against TGN46 and Sac1, GST-tagged fragments of human TGN46 (aa 1–365) and Sac1 (aa 1–55), respectively, were expressed in *Escherichia coli*, purified, and used as antigens. These antibodies were isolated by affinity chromatography on antigen-coupled beads. Polyclonal antibodies against VAP-A and Bap31 were produced as described previously (Wakana et al., 2008, 2015). An anti–mannosidase II polyclonal antibody was provided by V. Malhotra (Centre for Genomic Regulation, Barcelona, Spain). D/D solubilizer was purchased from Clontech. Methyl-β-cyclodextrin and 2-hydroxypropyl-β-cyclodextrin were purchased from FUJIFILM Wako Pure Chemical Corporation. Filipin and 25-HC were purchased from Sigma-Aldrich.

Plasmids

The plasmids encoding PAUF-MycHis, NA-GFP, Myc-OSBP (Nishimura et al., 2013), HA-CERT (Kumagai et al., 2007, 2014), and VSV-G–GFP were kindly donated by S.S. Koh (Korea Research Institute of Bioscience and Biotechnology, Daejeon, Korea), N. Nakamura (Kyoto Sangyo University, Kyoto, Japan), H. Arai (University of Tokyo, Tokyo, Japan), K. Hanada (National Institute of Infectious Diseases, Tokyo, Japan), and J. Lippincott-Schwartz (National Institutes of Health, Bethesda, MD), respectively. The plasmids encoding mKate2-FM4-GPI and EQ-SM (tagged with oxGFP) were generous gifts from C.G. Burd (Yale School of Medicine, New Haven, CT). The plasmids encoding the GFP-Sac1 WT and K2A mutant were generous gifts from P. Mayinger (Oregon Health and Science University, Portland, OR). The plasmids encoding FLAG-SREBP1a and FLAG-SREBP2 were generous gifts from D.M. Sabatini (Whitehead Institute for Biomedical Research, Cambridge, MA; Addgene plasmids #32017 and #32018; Peterson et al., 2011).

Downloaded from http://rupress.org/jcb/article-pdf/220/1/e202002150/1617891/jcb_202002150.pdf by guest on 06 May 2026

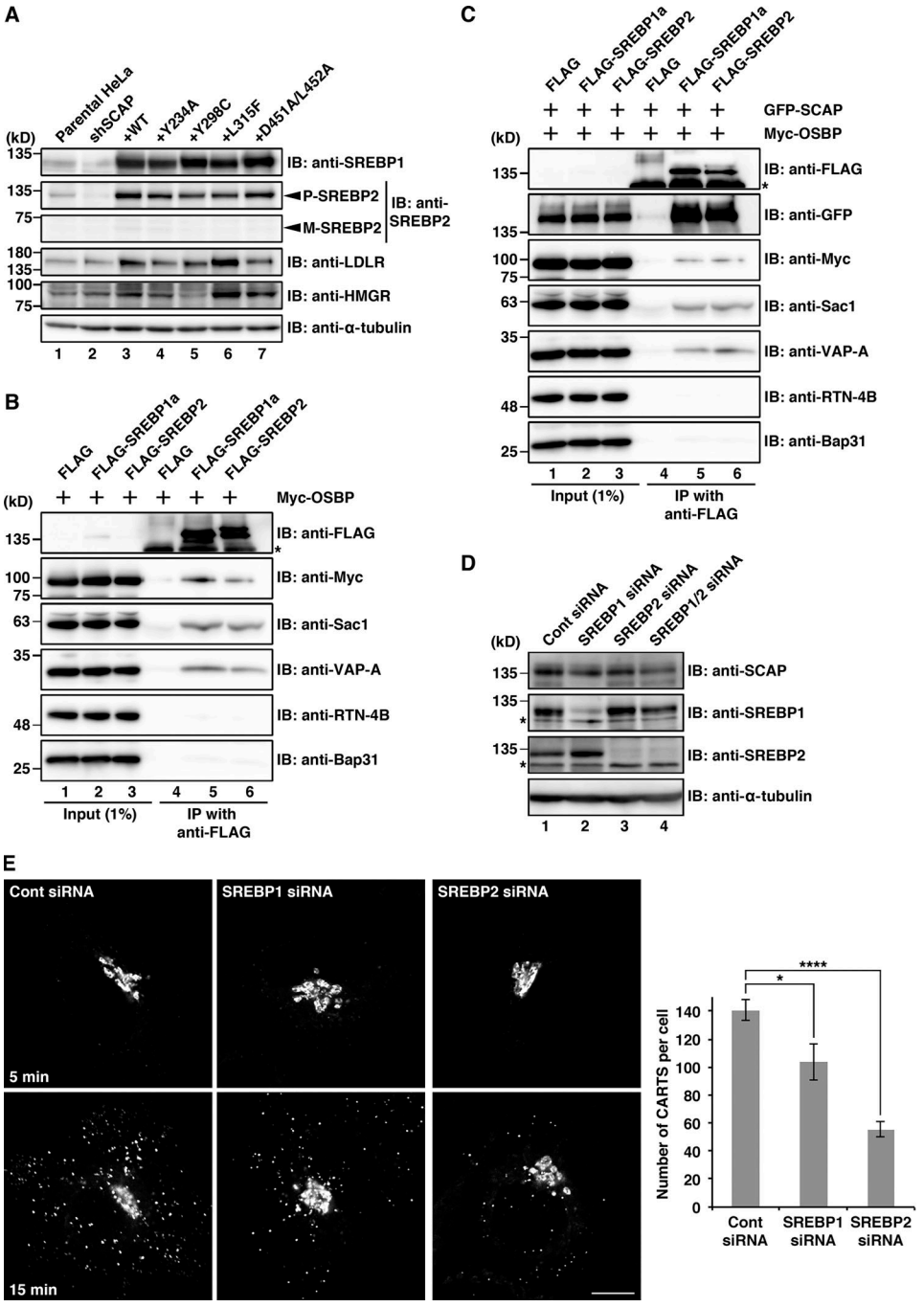

Figure 9. **The SCAP–SREBP complex functions in CARTS biogenesis. (A)** Effects of SCAP knockdown and expression of the hamster SCAP WT or mutants on the expression levels of SREBP1 and SREBP2. The precursor (P), but not the mature (M), form of SREBP2 was detected in parental HeLa cells and shSCAP HeLa cells stably expressing the hamster SCAP WT or mutants. Expression levels of LDLR and HMGR were significantly increased by expression of the L315F mutant. **(B)** Interactions of FLAG-SREBP1a and FLAG-SREBP2 with Myc-OSBP, Sac1, and VAP-A, but not with RTN-4B or Bap31, in HEK 293T cells. **(C)** Interactions of FLAG-SREBP1a and FLAG-SREBP2 with GFP-SCAP, Myc-OSBP, Sac1, and VAP-A, but not with RTN-4B or Bap31. **(D)** siRNA-mediated knockdown of SREBP1 and/or SREBP2 in HeLa cells. Asterisks in B–D denote nonspecific bands. **(E)** Biogenesis of mKate2-FM4-PAUF–containing CARTS in control (Cont), SREBP1, and SREBP2 knockdown cells. The graph shows the number of mKate2-FM4-PAUF–containing CARTS in the indicated cells at 15 min after the temperature shift to 37°C. Data are means ± SEM (n = 11 cells per condition; * P, < 0.05; ****, P < 0.0001; one-way ANOVA multiple comparison test). Scale bar, 10 µm. IB, immunoblotted; IP immunoprecipitate.

The plasmid encoding GST-PKD2-KD was provided by V. Malhotra (Centre for Genomic Regulation, Barcelona, Spain). The cDNAs encoding hamster SCAP WT and C-term (aa 732–1276) were amplified by PCR from pCMV-GFP-SCAP, a generous gift from P.J. Espenshade (Johns Hopkins University School of Medicine, Baltimore, MD), and inserted into pFLAG-CMV-6c to express the protein with an N-terminal FLAG. For expression of FLAG-SCAP D451A/L452A, point mutations were introduced

Downloaded from http://rupress.org/jcb/article-pdf/220/1/e202002150/1617891/jcb_202002150.pdf by guest on 06 May 2026

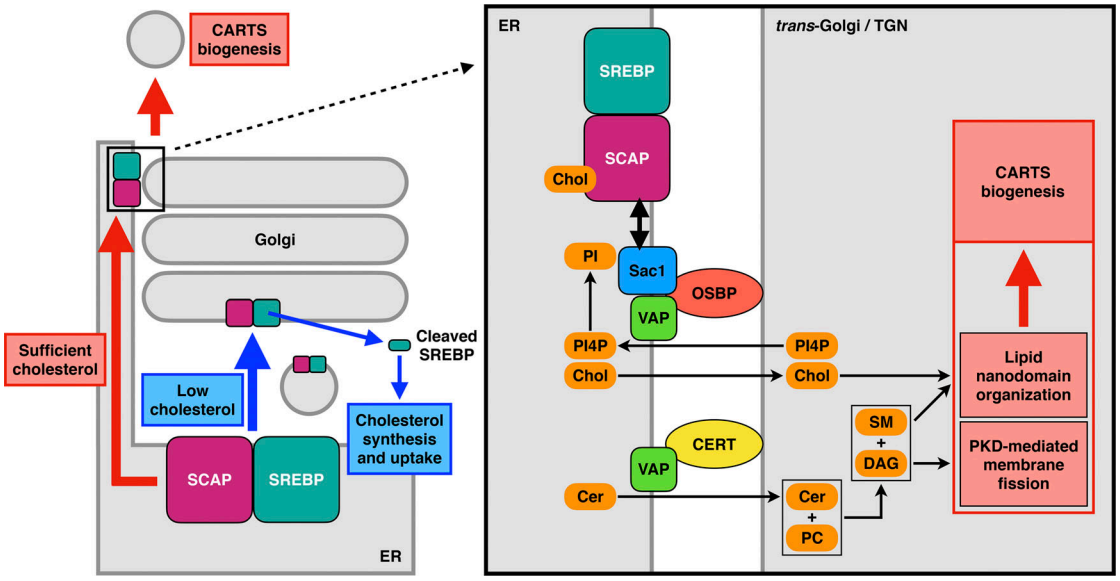

Figure 10. **Working model for the facilitation of CARTS biogenesis by the SCAP–SREBP complex at ER–Golgi MCSs.** Low cholesterol (Chol) levels: SCAP escorts SREBP transcription factors from the ER to the Golgi complex for cholesterol synthesis and uptake (left panel, blue arrows). Sufficient cholesterol levels: a complex of cholesterol-bound SCAP and SREBP interacts with the VAP–OSBP complex via Sac1 and functions in the counter-transport of ER cholesterol and Golgi PI4P at ER–Golgi MCSs to promote CARTS biogenesis at the TGN domains immediately adjacent to the ER MSCs (left panel, red arrows, and right panel). PC, phosphatidylcholine.

into pFLAG-SCAP by PCR using primers designed for replacing aspartic acid 451 and leucine 452 with alanines. The cDNA encoding hamster SCAP or rabbit OSBP (WT or FF/AA) was inserted into pCI-IRES-Bsr in combination with one encoding the Vn (aa 1–172). The cDNA encoding human Sac1 or VAP-A was inserted into pCI-IRES-Bsr in combination with one encoding the Vc (aa 154–238). For establishment of stable cell lines, the cDNAs encoding Vn-OSBP and Vc-VAP-A were inserted into the pMXs-IRES-Puro and pCX4-IRES-Bsr retroviral vectors, respectively, and hamster SCAP with or without N-terminal FLAG or GFP was inserted into pCX4-IRES-Bsr. For expression of SCAP Y234A, Y298C, L315F, D443N, or D451A/L452A, each point mutation was introduced into pCX4-SCAP-IRES-Bsr by PCR using primers designed for the purpose. For expression of mKate2-FM4-PAUF, the cDNA encoding GPI in the plasmid for mKate2-FM4-GPI was replaced with one encoding human PAUF (aa 55–208). The cDNA encoding human sialyltransferase (aa 1–69) was inserted into a pcDNA3-based plasmid encoding monomeric RFP (mRFP) to express the protein with a C-terminal mRFP. Plasmids for Myc-OSBP FF/AA and PH-FFAT were described previously (Wakana et al., 2015). For establishment of shSCAP HeLa cells, the Mission shRNA plasmid (TRCN0000289279) was purchased from Sigma-Aldrich.

siRNA and shRNA

The targeting sequences of siRNA and shRNA were as follows: control (GL2 luciferase): 5′-AACGTACGCGGAATACTTCGA-3′; SCAP (siRNA): 5′-AACCTCCTGGCAGTAGATGTA-3′; SCAP (shRNA): 5′-GCTCTGGTGTTCTTGGACAAA-3′; VAP-A: 5′-AACTAATGGAAGAGTGTAAAA-3′; VAP-B: 5′-AAGAAGGTTATGGAAGAATGT-3′; OSBP: 5′-AATACTGGGAGTGTAAAGAAA-3′; CERT: 5′-AAGAACAGAGGAAGCATATAA-3′; Sac1: 5′-AACTGATATTCAGTTACAAGA-3′; SREBP1: 5′-GAGGCAAAGCTGAATAAATCT-3′; and SREBP2: 5′-CAGGCTTTGAAGACGAAGCTA-3′.

Cell culture and transfection

HeLa and HEK 293T cells were grown in DMEM supplemented with 10% FCS. PLAT-A packaging cells were grown in DMEM supplemented with 10% FCS, 10 µg/ml blasticidin S, and 1 µg/ml puromycin. Plasmid and siRNA transfection into HeLa cells was performed using X-tremeGENE 9 DNA transfection reagent (Roche) and Oligofectamine reagent (Thermo Fisher Scientific), respectively, according to the manufacturers' protocols. Plasmid transfection into HEK 293T and PLAT-A packaging cells was performed using polyethylenimine (Polysciences) or Lipofectamine 2000 transfection reagent (Thermo Fisher Scientific).

Establishment of stable cell lines

For establishment of HeLa cells stably expressing FLAG- or GFP-SCAP, PLAT-A packaging cells were transfected with pCX4-FLAG- or GFP-SCAP-IRES-Bsr, and 48 h later, the medium containing retrovirus was collected and used for infection of HeLa cells. Selection of HeLa cells stably expressing FLAG- or GFP-SCAP was performed with 10 µg/ml blasticidin S. The expression level of FLAG-SCAP was estimated by Western blotting of cell lysates with an antibody specific to hamster SCAP and one recognizing both hamster and human SCAP. A HeLa stable cell line coexpressing Vn-OSBP and Vc-VAP-A was established in a similar manner with pMXs-Vn-OSBP-IRES-Puro and pCX4-Vc-VAP-A–IRES-Bsr by selecting cells with 1 µg/ml puromycin and 10 µg/ml blasticidin S. For establishment of shSCAP HeLa cells, HEK 293T cells were cotransfected with the Mission shRNA plasmid (TRCN0000289279), pMDLg/pRRE, pRSV-Rev, and pCMV–VSV-G. After 48 h, the medium containing lentivirus was

Downloaded from http://rupress.org/jcb/article-pdf/220/1/e202002150/1617891/jcb_202002150.pdf by guest on 06 May 2026

collected and used for infection of HeLa cells. Selection of shSCAP HeLa cells was performed with 1 µg/ml puromycin. Establishment of shSCAP HeLa cells stably expressing hamster SCAP WT, Y234A, Y298C, L315F, D443N, or D451A/L452A was performed with pCX4-SCAP (WT or mutants)-IRES-Bsr as described for FLAG- or GFP-SCAP HeLa cells. All the stable cell lines were obtained without single-cell cloning.

Immunofluorescence microscopy

HeLa cells were fixed with 4% PFA in PBS at room temperature for 20 min, permeabilized with 0.2% Triton X-100 in PBS for 30 min, and then blocked with 2% BSA in PBS for 30 min. The cells were labeled with the indicated primary antibodies and secondary antibodies conjugated to Alexa Fluor 488, 594, 633, or 647 in the blocking buffer. The samples were analyzed with an Olympus Fluoview FV1000 or FV1200 confocal microscope with a UPLSAPO 60× O NA 1.35 objective and FV10-ASW software. Image processing and measurement of fluorescence intensity were performed with ImageJ software (National Institutes of Health). Vesicular structures containing EQ-SM and/or PAUF-MycHis were detected using the plugin ComDet (https://github.com/ekatrukha/ComDet).

Image deconvolution

Deconvolution processing was performed with Huygens Professional version 18.04 (Scientific Volume Imaging, Netherlands; http://svi.nl). For that, a theoretical point-spread function was automatically computed based on the microscope and image acquisition parameters. The deconvolution process was numerically performed using the Classic Maximum Likelihood Estimation algorithm. In brief, this algorithm assumes that the photon noise is Poisson-distributed, and the likelihood of an estimate of the actual image given the computed point-spread function and the acquired image is iteratively optimized until either a quality factor or a maximum number of iterations is reached. In our deconvolutions, we used a quality factor equal to 0.001 and a maximum 50 iterations. The signal-to-noise ratio for each acquired image was computed based on three line profiles going through regions of background signals toward regions of positive, actual signals. Typically, signal-to-noise ratios were on the order of 7–20 for the different analyzed confocal images and 7 for the STED image.

Visualization of PAUF-MycHis by STED microscopy

For STED imaging, HeLa cells stably coexpressing Vn-OSBP and Vc-VAP-A were seeded on #1.5H–thickness cover glasses (ThorLabs) and transfected with a plasmid for PAUF-MycHis. After 20 h, the cells were treated with 2 µg/ml 25-HC for 2.5 h, after which they were fixed and processed as indicated for immunofluorescence microscopy. To image PAUF-MycHis using STED, we used a mouse anti-Myc (clone 9E10) primary antibody (1:200 dilution) and an Abberior STAR 635P–conjugated goat anti-mouse IgG secondary antibody (10 µg/ml). The cover glasses were mounted on glass slides using ProLong Gold (Thermo Fisher Scientific). Images were obtained on a commercial Leica TCS SP8 STED 3× microscope equipped with a pulsed supercontinuum white light laser excitation source, using a 100× 1.4 NA oil HC PL APO CS2 objective. The BiFC signal was detected in confocal mode (no STED) using 514-nm wavelength excitation at 8% of the white-light laser intensity (set at 70% output power); the PAUF-MycHis signal was detected in STED mode, where the excitation was done using a 633-nm line at 1% of the white-light laser intensity and the depletion was performed with a second ps-pulsed laser at 775 nm with a 0-ps pulse delay and used at 100% intensity (output power set to 100%). The two channels were imaged sequentially line by line, in an almost simultaneous manner to minimize the effects of mechanical drift of the system. Images were taken with 16× line accumulation in a 19.37 × 19.37–µm field of view (1,816 × 1,816 pixels) with a pixel size of 10.7 nm, with unidirectional scanning at 400 lines per second. The detection of the two channels was done with two separate HyD SMD detectors in photon counting mode and acquisition windows set to 524–607 nm (for the BiFC channel) and to 643–745 nm (for the PAUF-MycHis channel) and using time gating (gating from 0.3 ns to 6 ns). With these settings, the effective optical resolution obtained was ∼30 nm for the PAUF-MycHis channel. Images were acquired with the Leica LAS AF software and further deconvolved using Huygens software, as detailed in the image deconvolution section, to improve the spatial resolution in both the confocal BiFC channel and the STED PAUF-MycHis channel.

Filipin staining

Filipin staining was performed as described previously (Wilhelm et al., 2017). In brief, HeLa cells were treated with 10 mM methyl-β-cyclodextrin at 37°C for 30 min and fixed with 4% PFA at room temperature for 10 min. The cells were incubated with 0.1 mg/ml filipin in PBS at room temperature for 30 min. After washing with PBS, the cells were blocked with 1% BSA in PBS for 30 min and labeled with an anti–Golgin-97 antibody and a secondary antibody conjugated to Alexa Fluor 594 in the blocking buffer. After reincubation with 0.1 mg/ml filipin at room temperature for 30 min, the cells were washed with PBS and then mounted on a microscope slide. The samples were analyzed by fluorescence microscopy as described above.

PI4P staining

PI4P staining was performed as described previously (Hammond et al., 2009; Capasso et al., 2017). In brief, HeLa cells were fixed with 2% PFA at room temperature for 15 min, followed by washing with PBS containing 50 mM NH_4Cl. The cells were then permeabilized with 20 µM digitonin in buffer A (20 mM Pipes-NaOH, pH 6.8, 137 mM NaCl, and 2.7 mM KCl) for 5 min. After removal of digitonin by washing with buffer A, the cells were blocked with 5% FCS in buffer A for 45 min. The cells were labeled with anti-PI4P and anti–Golgin-97 antibodies, followed by secondary antibodies conjugated to Alexa Fluor 488 and 594, respectively, in the blocking buffer. After fixation with 2% PFA for 5 min, the cells were washed with PBS containing 50 mM NH_4Cl and with water and then mounted on a microscope slide. The samples were analyzed by fluorescence microscopy as described above.

Quantification of Golgi PI4P

To quantify the intensity of the PI4P signal at the Golgi complex from our immunofluorescence microscopy images, we used the

Downloaded from http://rupress.org/jcb/article-pdf/220/1/e202002150/1617891/jcb_202002150.pdf by guest on 06 May 2026

ImageJ distribution Fiji (Schindelin et al., 2012) and a custom-made macro, following the method described in the paper by Venditti et al. (2019). First, we generated a binary mask for the Golgi/TGN area using the signal of the marker protein Golgin-97 after 1-pixel radius Gaussian blur filtering. Then, the mean intensities of the PI4P and Golgin-97 channels in the Golgi/TGN mask areas were background subtracted and measured separately for each individual cell. Finally, the measured Golgi (mask) PI4P levels were normalized to the Golgi (mask) Golgin-97 levels for each cell.

Quantification of perinuclear BiFC signal

To quantify the perinuclear BiFC signal from our fluorescence microscopy images, we used Fiji and a custom-made macro. First, we generated a binary mask for the perinuclear area using the signal of the TGN marker protein TGN46 after 1-pixel radius Gaussian blur filtering. Finally, the total intensity of the BiFC channel in the perinuclear mask area was measured separately for each individual cell after background subtraction.

iFRAP

HeLa cells expressing GFP-Sac1 WT, K2A, or NA-GFP in Opti-MEM were cultured in 5% CO_2 at 37°C during live-cell imaging. The cells were subjected to bleaching with high laser intensity (473-nm laser) for 15 s, followed by an imaging scan with a time interval between frames of 10 s for ∼4 min by use of an Olympus Fluoview FV1000 confocal microscope with a UPLSAPO 100× O NA 1.40 objective and FV10-ASW software. Image processing and measurement of fluorescence intensity were performed with ImageJ software.

Immunoprecipitation

HEK 293T cells were lysed in buffer B (50 mM Hepes-KOH, pH 7.4, 100 mM NaCl, 1.5 mM $MgCl_2$, 1 mM dithiothreitol, 1% Nonidet P-40, 1 µg/ml leupeptin, 2 µM pepstatin A, 2 µg/ml aprotinin, and 1 mM phenylmethylsulfonyl fluoride). The lysates were centrifuged at 17,400× *g* for 10 min. The resulting supernatants were immunoprecipitated with an anti-FLAG M2 affinity gel (Sigma-Aldrich), and the precipitated proteins were analyzed by Western blotting with the indicated primary antibodies and secondary antibodies conjugated to horseradish peroxidase. For immunoprecipitation of FLAG-SREBPs, stably expressed FLAG-SCAP, or endogenous Sac1, cells were lysed in buffer B without dithiothreitol, and the lysates were centrifuged at 17,400× *g* for 10 min. The supernatants were further centrifuged at 100,000× *g* for 30 min, and the resulting supernatants were immunoprecipitated with an anti-FLAG M2 affinity gel or Dynabeads Protein G (Thermo Fisher Scientific) coupled with control rabbit IgG or an anti-Sac1 antibody. For identification of Sac1 interacting proteins, the precipitated proteins were eluted with FLAG peptide and analyzed by silver staining. Protein bands were excised from the gel and subjected to liquid chromatography–tandem mass spectrometry (LC-MS/MS) analysis.

LC-MS/MS analysis

Each gel piece was incubated with 0.25 µg trypsin in 20 µl Tris-HCl, pH 8.8, overnight at 37°C (Taoka et al., 2000), and the resulting peptide mixture was analyzed with a direct nanoflow LC-MS/MS system equipped with a hybrid quadrupole-orbitrap mass spectrometer (Q Exactive; Thermo Fisher Scientific) as previously described (Taoka et al., 2014). Briefly, peptides were separated on a reversed-phase tip column (150 µm i.d. × 70 mm; Mightysil-C18; 3-µm particle) using a 0–35% linear gradient of acetonitrile in 0.1% (vol/vol) formic acid for 35 or 70 min at a flow rate of 100 nl/min. Full MS scans were acquired with a resolution of 30,000 at a mass-to-charge ratio of 400. The 10 most intense ions were fragmented in the data-dependent mode by collision-induced dissociation with normalized collision energy of 35, activation q of 0.25, and activation time of 10 ms and one microscan. The MS/MS data were converted to the Mascot generic format with Proteome Discoverer software (version 1.1; Thermo Fisher Scientific). The files were processed with the Mascot algorithm (version 2.2.1; Matrix Science Ltd.) to assign peptides using the Swiss-Prot sequence database (release 2012.11, human) under the search parameters described in the paper by Taoka et al. (2014). Peptides were identified based on the Mascot definitions. For the search parameters, we set the variable modifications for acetylation (protein N-terminus) and oxidation (Met). The maximum missed cleavage was set at 1 with a peptide mass tolerance of ±15 ppm. Peptide charges from +2 to +4 states and MS/MS tolerances of ±0.8 D were allowed. All results of peptide searches were extracted from the Mascot DAT files using STEM software (Shinkawa et al., 2005).

Cholesterol depletion

Lipoprotein-deficient serum was prepared as described previously (Goldstein et al., 1983; Poumay and Ronveaux-Dupal, 1985). In brief, FCS was adjusted to a density of 1.25 g/ml with solid KBr and then centrifuged for 16 h at 10°C at 50,000 rpm in a Beckman VTi 50 rotor. The upper yellow-orange layer containing lipoproteins and the salt pellet were removed, and the remaining fraction was dialyzed extensively at 4°C against 150 mM NaCl for 48 h. HeLa cells were incubated with DMEM containing 5% lipoprotein-deficient serum and 1% 2-hydroxypropyl-β-cyclodextrin for 3 h.

Quantitative real-time PCR

RNA was prepared using an RNeasy Mini kit (Qiagen), and cDNA was synthesized with SuperScript III reverse transcription (Thermo Fisher Scientific) primed by oligo(dT)15. Quantitative real-time PCR was performed with a Rotor-Gene Q RT-PCR machine (Qiagen) using a KAPA SYBR FAST qPCR Kit (Kapa Biosystems), according to the manufacturer's protocol. The primers used were as follows: SCAP, forward primer 5′-TATCTCGGGCCT TCTACAACC-3′ and reverse primer 5′-GGGGCGAGTAATCCTTCA CA-3′; HMGR, forward primer 5′-TGACCTTTCCAGAGCAAGC-3′ and reverse primer 5′-CCAACTCCAATCACAAGACATTC-3′; LDLR, forward primer 5′-GTGTCACAGCGGCGAATG-3′ and reverse primer 5′-CGCACTCTTTGATGGGTTCA-3′; HPRT1, forward primer 5′-TTCCAGACAAGTTTGTTGTAGGAT-3′ and reverse primer 5′-GCAGATGGCCACAGAACTAG-3′. Values were normalized as the HPRT1 expression level.

Total cholesterol measurement

HeLa cells were lysed in water for 30 min at 37°C and then subjected to total cholesterol measurement with an Amplex Red

Downloaded from http://rupress.org/jcb/article-pdf/220/1/e202002150/1617891/jcb_202002150.pdf by guest on 06 May 2026

cholesterol assay kit (Thermo Fisher Scientific) according to the manufacturer's protocol. Values were normalized to protein content determined by using a Pierce BCA protein assay kit (Thermo Fisher Scientific).

PAUF secretion assay

HeLa cells were transfected with control siRNA or siRNA oligos targeting SCAP. At 48 h after siRNA transfection, the cells were transfected with a plasmid for PAUF-MycHis; 20 h later, the medium was replaced with Opti-MEM, and then the cells were incubated at 37°C for 6 h. After the medium was collected, the cells were lysed with 0.5% SDS and 0.025 U/µl benzonase nuclease (Sigma-Aldrich) in PBS. The medium and cell lysates were analyzed by Western blotting with an anti–Penta-His antibody.

GPI transport assay

HeLa cells were transfected with control siRNA or siRNA oligos targeting SCAP, VAP-A/B, OSBP, or CERT/OSBP. At 48 h after siRNA transfection, the cells were transfected with a plasmid for mKate2-FM4-GPI; 20 h later, the medium was replaced with DMEM containing 10% FCS, 1 µM D/D solubilizer, and 20 µg/ml cycloheximide, and then the cells were incubated at 37°C for the indicated times. The cells were then fixed with 4% PFA and analyzed by fluorescence microscopy as described above.

Inducible CARTS formation assay

HeLa cells were transfected with control siRNA or siRNA oligos targeting SCAP, SREBP1, or SREBP2. At 48 h after siRNA transfection, the cells were transfected with a plasmid for mKate2-FM4-PAUF; 20 h later, the medium was replaced with DMEM containing 10% FCS, 20 mM Hepes-KOH, pH 7.4, 1 µM D/D solubilizer, and 20 µg/ml cycloheximide, and then the cells were incubated in a water bath at 20°C for 45 min. The cells were then incubated in a water bath at 37°C for 5 or 15 min, followed by fixation with 4% PFA. The samples were analyzed by fluorescence microscopy as described above. Quantification of CARTS was performed with ImageJ software. The fluorescence signal of mKate2-FM4-PAUF–containing puncta was distinguished from the background by setting a threshold and was analyzed at a set size within 0.05–2.00 µm^2. For live-cell imaging, HeLa cells were transfected with a plasmid for mKate2-FM4-PAUF; 20 h later, the medium was replaced with Opti-MEM containing 1 µM D/D solubilizer and 20 µg/ml cycloheximide, and then the cells were incubated in a water bath at 20°C for 45 min. The cells were then incubated at 37°C and 5% CO_2 to monitor CARTS biogenesis. Images were acquired continuously with a time interval between frames of 30 s for ∼75 min by use of an Olympus Fluoview FV1200 confocal microscope with a UPLSAPO 60× O NA 1.35 objective and FV10-ASW software. The images were processed with ImageJ software.

VSV-G transport assay

HeLa cells were transfected with control siRNA or siRNA oligos targeting SCAP. At 48 h after siRNA transfection, the cells were transfected with a plasmid for VSV-G–GFP. After incubation at 40°C for 18 h, the medium was replaced with DMEM containing 10% FCS, 20 mM Hepes-KOH, pH 7.4, and 20 µg/ml cycloheximide, and then the cells were incubated in a water bath at 32°C to allow transport from the ER to the PM through the Golgi complex. The cells were then fixed with 4% PFA at the indicated times and analyzed by fluorescence microscopy as described above.

Online supplemental material

Fig. S1 shows colocalization of GFP-Sac1 WT or K2A with VAP-A and their proximity to Golgi markers in cells treated with or without nocodazole. Fig. S2 shows additional results related to Fig. 3, in which Vn- or Vc-fused constructs were evaluated for BiFC analysis. Fig. S3 shows the localization of GFP- or non-tagged SCAP WT or mutants in cells with or without cholesterol depletion or treated with 25-HC. Fig. S4 shows experiments related to Fig. 5, in which PI4P was visualized in control cells and cells depleted of components of ER–Golgi MCSs, and the VAP-A–OSBP complex was visualized by BiFC in a stable cell line. Fig. S5 shows GPI-anchored protein transport in control cells and cells where functions of ER–Golgi MCSs were perturbed, and VSV-G transport in control and SCAP knockdown cells. Video 1 shows the kinetics of biogenesis of mKate2-FM4-PAUF–containing CARTS at the TGN.

Acknowledgments

We thank Peter J. Espenshade, Peter Mayinger, Hiroyuki Arai, Kentaro Hanada, Nobuhiro Nakamura, Sang Seok Koh, David M. Sabatini, Christopher G. Burd, Jennifer Lippincott-Schwartz, and Vivek Malhotra for providing materials. We appreciate the technical assistance of Nanako Oyama, So Yoshida, Yurika Komatsuda, Yuiko Kawai, Natsumi Hoshino, Tomoya Iizuka, Sho Furuichi, and Katsunori Iwasa.

This work was supported in part by Grants-in-Aid for Scientific Research from the Ministry of Education, Culture, Sports, Science, and Technology of Japan (grants 15K18507 and 17K07348 to Y. Wakana and 18H02439 to M. Tagaya), the Naito Foundation (to Y. Wakana), and the Ono Medical Research Foundation (to Y. Wakana). We acknowledge support from the Government of Spain (FIS2017-89560-R, BFU2015-73288-JIN, RYC-2017-22227, and PID2019-106232RB-I00/10.13039/501100011033; Severo Ochoa CEX2019-000910-S), Fundació Cellex, Fundació Mir-Puig, and Generalitat de Catalunya (Centres de Recerca de Catalunya and Agència de Gestió d'Ajuts Universitaris i de Recerca; to J. Angulo-Capel, M.F. Garcia-Parajo, and F. Campelo). This project has received funding from the European Union's Horizon 2020 research and innovation program under Marie Skłodowska-Curie grant agreement number 847517 (to J. Angulo-Capel).

The authors declare no competing financial interests.

Author contributions: Y. Wakana and M. Tagaya conceived and designed the experiments. Y. Wakana, K. Hayashi, T. Nemoto, C. Watanabe, J. Angulo-Capel, H. Kumata, and F. Campelo performed the experiments. Y. Wakana, J. Angulo-Capel, and F. Campelo performed the image analyses. M. Taoka performed the LC-MS/MS analysis. M.F. Garcia-Parajo, T. Umemura, H. Inoue, K. Arasaki, and M. Tagaya provided samples. Y. Wakana and M. Tagaya wrote the manuscript.

Downloaded from http://rupress.org/jcb/article-pdf/220/1/e202002150/1617891/jcb_202002150.pdf by guest on 06 May 2026

Submitted: 26 February 2020
Revised: 15 September 2020
Accepted: 12 October 2020

References

Adams, C.M., J.L. Goldstein, and M.S. Brown. 2003. Cholesterol-induced conformational change in SCAP enhanced by Insig proteins and mimicked by cationic amphiphiles. *Proc. Natl. Acad. Sci. USA.* 100:10647–10652. https://doi.org/10.1073/pnas.1534833100

Adams, C.M., J. Reitz, J.K. De Brabander, J.D. Feramisco, L. Li, M.S. Brown, and J.L. Goldstein. 2004. Cholesterol and 25-hydroxycholesterol inhibit activation of SREBPs by different mechanisms, both involving SCAP and Insigs. *J. Biol. Chem.* 279:52772–52780. https://doi.org/10.1074/jbc.M410302200

Antonny, B., J. Bigay, and B. Mesmin. 2018. The Oxysterol-Binding Protein Cycle: Burning Off PI(4)P to Transport Cholesterol. *Annu. Rev. Biochem.* 87:809–837. https://doi.org/10.1146/annurev-biochem-061516-044924

Baron, C.L., and V. Malhotra. 2002. Role of diacylglycerol in PKD recruitment to the TGN and protein transport to the plasma membrane. *Science.* 295:325–328. https://doi.org/10.1126/science.1066759

Blagoveshchenskaya, A., F.Y. Cheong, H.M. Rohde, G. Glover, A. Knödler, T. Nicolson, G. Boehmelt, and P. Mayinger. 2008. Integration of Golgi trafficking and growth factor signaling by the lipid phosphatase SAC1. *J. Cell Biol.* 180:803–812. https://doi.org/10.1083/jcb.200708109

Brown, M.S., and J.L. Goldstein. 1997. The SREBP pathway: regulation of cholesterol metabolism by proteolysis of a membrane-bound transcription factor. *Cell.* 89:331–340. https://doi.org/10.1016/S0092-8674(00)80213-5

Brown, D.A., and J.K. Rose. 1992. Sorting of GPI-anchored proteins to glycolipid-enriched membrane subdomains during transport to the apical cell surface. *Cell.* 68:533–544. https://doi.org/10.1016/0092-8674(92)90189-J

Brown, A.J., L. Sun, J.D. Feramisco, M.S. Brown, and J.L. Goldstein. 2002. Cholesterol addition to ER membranes alters conformation of SCAP, the SREBP escort protein that regulates cholesterol metabolism. *Mol. Cell.* 10:237–245. https://doi.org/10.1016/S1097-2765(02)00591-9

Brown, M.S., A. Radhakrishnan, and J.L. Goldstein. 2018. Retrospective on Cholesterol Homeostasis: The Central Role of Scap. *Annu. Rev. Biochem.* 87:783–807. https://doi.org/10.1146/annurev-biochem-062917-011852

Campelo, F., J. van Galen, G. Turacchio, S. Parashuraman, M.M. Kozlov, M.F. García-Parajo, and V. Malhotra. 2017. Sphingomyelin metabolism controls the shape and function of the Golgi cisternae. *eLife.* 6:e24603. https://doi.org/10.7554/eLife.24603

Capasso, S., L. Sticco, R. Rizzo, M. Pirozzi, D. Russo, N.A. Dathan, F. Campelo, J. van Galen, M. Hölttä-Vuori, G. Turacchio, et al. 2017. Sphingolipid metabolic flow controls phosphoinositide turnover at the *trans*-Golgi network. *EMBO J.* 36:1736–1754. https://doi.org/10.15252/embj.201696048

Cheong, F.Y., V. Sharma, A. Blagoveshchenskaya, V.M.J. Oorschot, B. Brankatschk, J. Klumperman, H.H. Freeze, and P. Mayinger. 2010. Spatial regulation of Golgi phosphatidylinositol-4-phosphate is required for enzyme localization and glycosylation fidelity. *Traffic.* 11:1180–1190. https://doi.org/10.1111/j.1600-0854.2010.01092.x

Cole, N.B., N. Sciaky, A. Marotta, J. Song, and J. Lippincott-Schwartz. 1996. Golgi dispersal during microtubule disruption: regeneration of Golgi stacks at peripheral endoplasmic reticulum exit sites. *Mol. Biol. Cell.* 7:631–650. https://doi.org/10.1091/mbc.7.4.631

De Matteis, M.A., A. Di Campli, and A. Godi. 2005. The role of the phosphoinositides at the Golgi complex. *Biochim. Biophys. Acta.* 1744:396–405. https://doi.org/10.1016/j.bbamcr.2005.04.013

Deng, Y., F.E. Rivera-Molina, D.K. Toomre, and C.G. Burd. 2016. Sphingomyelin is sorted at the *trans* Golgi network into a distinct class of secretory vesicle. *Proc. Natl. Acad. Sci. USA.* 113:6677–6682. https://doi.org/10.1073/pnas.1602875113

Deng, Y., M. Pakdel, B. Blank, E.L. Sundberg, C.G. Burd, and J. von Blume. 2018. Activity of the SPCA1 Calcium Pump Couples Sphingomyelin Synthesis to Sorting of Secretory Proteins in the Trans-Golgi Network. *Dev. Cell.* 47:464–478.e8: E8. https://doi.org/10.1016/j.devcel.2018.10.012

Dippold, H.C., M.M. Ng, S.E. Farber-Katz, S.-K. Lee, M.L. Kerr, M.C. Peterman, R. Sim, P.A. Wiharto, K.A. Galbraith, S. Madhavarapu, et al. 2009. GOLPH3 bridges phosphatidylinositol-4- phosphate and actomyosin to stretch and shape the Golgi to promote budding. *Cell.* 139:337–351. https://doi.org/10.1016/j.cell.2009.07.052

Dong, R., Y. Saheki, S. Swarup, L. Lucast, J.W. Harper, and P. De Camilli. 2016. Endosome-ER Contacts Control Actin Nucleation and Retromer Function through VAP-Dependent Regulation of PI4P. *Cell.* 166:408–423. https://doi.org/10.1016/j.cell.2016.06.037

Duran, J.M., F. Campelo, J. van Galen, T. Sachsenheimer, J. Sot, M.V. Egorov, C. Rentero, C. Enrich, R.S. Polishchuk, F.M. Goñi, et al. 2012. Sphingomyelin organization is required for vesicle biogenesis at the Golgi complex. *EMBO J.* 31:4535–4546. https://doi.org/10.1038/emboj.2012.317

Friedman, J.R., L.L. Lackner, M. West, J.R. DiBenedetto, J. Nunnari, and G.K. Voeltz. 2011. ER tubules mark sites of mitochondrial division. *Science.* 334:358–362. https://doi.org/10.1126/science.1207385

Fugmann, T., A. Hausser, P. Schöffler, S. Schmid, K. Pfizenmaier, and M.A. Olayioye. 2007. Regulation of secretory transport by protein kinase D-mediated phosphorylation of the ceramide transfer protein. *J. Cell Biol.* 178:15–22. https://doi.org/10.1083/jcb.200612017

Goldstein, J.L., S.K. Basu, and M.S. Brown. 1983. Receptor-mediated endocytosis of low-density lipoprotein in cultured cells. *Methods Enzymol.* 98:241–260. https://doi.org/10.1016/0076-6879(83)98152-1

Gomez-Navarro, N., and E. Miller. 2016. Protein sorting at the ER-Golgi interface. *J. Cell Biol.* 215:769–778. https://doi.org/10.1083/jcb.201610031

Gong, Y., J.N. Lee, M.S. Brown, J.L. Goldstein, and J. Ye. 2006. Juxtamembranous aspartic acid in Insig-1 and Insig-2 is required for cholesterol homeostasis. *Proc. Natl. Acad. Sci. USA.* 103:6154–6159. https://doi.org/10.1073/pnas.0601923103

Hammond, G.R.V., G. Schiavo, and R.F. Irvine. 2009. Immunocytochemical techniques reveal multiple, distinct cellular pools of PtdIns4*P* and PtdIns(4,5)P_2. *Biochem. J.* 422:23–35. https://doi.org/10.1042/BJ20090428

Hanada, K., K. Kumagai, S. Yasuda, Y. Miura, M. Kawano, M. Fukasawa, and M. Nishijima. 2003. Molecular machinery for non-vesicular trafficking of ceramide. *Nature.* 426:803–809. https://doi.org/10.1038/nature02188

Horton, J.D., N.A. Shah, J.A. Warrington, N.N. Anderson, S.W. Park, M.S. Brown, and J.L. Goldstein. 2003. Combined analysis of oligonucleotide microarray data from transgenic and knockout mice identifies direct SREBP target genes. *Proc. Natl. Acad. Sci. USA.* 100:12027–12032. https://doi.org/10.1073/pnas.1534923100

Hua, X., A. Nohturfft, J.L. Goldstein, and M.S. Brown. 1996. Sterol resistance in CHO cells traced to point mutation in SREBP cleavage-activating protein. *Cell.* 87:415–426. https://doi.org/10.1016/S0092-8674(00)81362-8

Ikonen, E. 2018. Mechanisms of cellular cholesterol compartmentalization: recent insights. *Curr. Opin. Cell Biol.* 53:77–83. https://doi.org/10.1016/j.ceb.2018.06.002

Jacobson, K., P. Liu, and B.C. Lagerholm. 2019. The Lateral Organization and Mobility of Plasma Membrane Components. *Cell.* 177:806–819. https://doi.org/10.1016/j.cell.2019.04.018

Kawano, M., K. Kumagai, M. Nishijima, and K. Hanada. 2006. Efficient trafficking of ceramide from the endoplasmic reticulum to the Golgi apparatus requires a VAMP-associated protein-interacting FFAT motif of CERT. *J. Biol. Chem.* 281:30279–30288. https://doi.org/10.1074/jbc.M605032200

Keller, P., and K. Simons. 1998. Cholesterol is required for surface transport of influenza virus hemagglutinin. *J. Cell Biol.* 140:1357–1367. https://doi.org/10.1083/jcb.140.6.1357

Kentala, H., S.G. Pfisterer, V.M. Olkkonen, and M. Weber-Boyvat. 2015. Sterol liganding of OSBP-related proteins (ORPs) regulates the subcellular distribution of ORP-VAPA complexes and their impacts on organelle structure. *Steroids.* 99(Pt B):248–258. https://doi.org/10.1016/j.steroids.2015.01.027

Klemm, R.W., C.S. Ejsing, M.A. Surma, H.-J. Kaiser, M.J. Gerl, J.L. Sampaio, Q. de Robillard, C. Ferguson, T.J. Proszynski, A. Shevchenko, and K. Simons. 2009. Segregation of sphingolipids and sterols during formation of secretory vesicles at the trans-Golgi network. *J. Cell Biol.* 185:601–612. https://doi.org/10.1083/jcb.200901145

Kumagai, K., and K. Hanada. 2019. Structure, functions and regulation of CERT, a lipid-transfer protein for the delivery of ceramide at the ER-Golgi membrane contact sites. *FEBS Lett.* 593:2366–2377. https://doi.org/10.1002/1873-3468.13511

Kumagai, K., M. Kawano, F. Shinkai-Ouchi, M. Nishijima, and K. Hanada. 2007. Interorganelle trafficking of ceramide is regulated by phosphorylation-dependent cooperativity between the PH and START domains of CERT. *J. Biol. Chem.* 282:17758–17766. https://doi.org/10.1074/jbc.M702291200

Kumagai, K., M. Kawano-Kawada, and K. Hanada. 2014. Phosphoregulation of the ceramide transport protein CERT at serine 315 in the interaction

Downloaded from http://rupress.org/jcb/article-pdf/220/1/e202002150/1617891/jcb_202002150.pdf by guest on 06 May 2026

with VAMP-associated protein (VAP) for inter-organelle trafficking of ceramide in mammalian cells. *J. Biol. Chem.* 289:10748–10760. https://doi.org/10.1074/jbc.M113.528380

Lavieu, G., L. Orci, L. Shi, M. Geiling, M. Ravazzola, F. Wieland, P. Cosson, and J.E. Rothman. 2010. Induction of cortical endoplasmic reticulum by dimerization of a coatomer-binding peptide anchored to endoplasmic reticulum membranes. *Proc. Natl. Acad. Sci. USA.* 107:6876–6881. https://doi.org/10.1073/pnas.1002536107

Liljedahl, M., Y. Maeda, A. Colanzi, I. Ayala, J. Van Lint, and V. Malhotra. 2001. Protein kinase D regulates the fission of cell surface destined transport carriers from the trans-Golgi network. *Cell.* 104:409–420. https://doi.org/10.1016/S0092-8674(01)00228-8

Liu, Y., M. Boukhelifa, E. Tribble, E. Morin-Kensicki, A. Uetrecht, J.E. Bear, and V.A. Bankaitis. 2008. The Sac1 phosphoinositide phosphatase regulates Golgi membrane morphology and mitotic spindle organization in mammals. *Mol. Biol. Cell.* 19:3080–3096. https://doi.org/10.1091/mbc.e07-12-1290

Loewen, C.J.R., A. Roy, and T.P. Levine. 2003. A conserved ER targeting motif in three families of lipid binding proteins and in Opi1p binds VAP. *EMBO J.* 22:2025–2035. https://doi.org/10.1093/emboj/cdg201

Malhotra, V., and F. Campelo. 2011. PKD regulates membrane fission to generate TGN to cell surface transport carriers. *Cold Spring Harb. Perspect. Biol.* 3:a005280. https://doi.org/10.1101/cshperspect.a005280

Matsuda, M., B.S. Korn, R.E. Hammer, Y.-A. Moon, R. Komuro, J.D. Horton, J.L. Goldstein, M.S. Brown, and I. Shimomura. 2001. SREBP cleavage-activating protein (SCAP) is required for increased lipid synthesis in liver induced by cholesterol deprivation and insulin elevation. *Genes Dev.* 15:1206–1216. https://doi.org/10.1101/gad.891301

Mayor, S., and H. Riezman. 2004. Sorting GPI-anchored proteins. *Nat. Rev. Mol. Cell Biol.* 5:110–120. https://doi.org/10.1038/nrm1309

Mesmin, B., J. Bigay, J. Moser von Filseck, S. Lacas-Gervais, G. Drin, and B. Antonny. 2013. A four-step cycle driven by PI(4)P hydrolysis directs sterol/PI(4)P exchange by the ER-Golgi tether OSBP. *Cell.* 155:830–843. https://doi.org/10.1016/j.cell.2013.09.056

Moon, Y.-A., G. Liang, X. Xie, M. Frank-Kamenetsky, K. Fitzgerald, V. Koteliansky, M.S. Brown, J.L. Goldstein, and J.D. Horton. 2012. The Scap/SREBP pathway is essential for developing diabetic fatty liver and carbohydrate-induced hypertriglyceridemia in animals. *Cell Metab.* 15:240–246. https://doi.org/10.1016/j.cmet.2011.12.017

Motamed, M., Y. Zhang, M.L. Wang, J. Seemann, H.J. Kwon, J.L. Goldstein, and M.S. Brown. 2011. Identification of luminal Loop 1 of Scap protein as the sterol sensor that maintains cholesterol homeostasis. *J. Biol. Chem.* 286:18002–18012. https://doi.org/10.1074/jbc.M111.238311

Nhek, S., M. Ngo, X. Yang, M.M. Ng, S.J. Field, J.M. Asara, N.D. Ridgway, and A. Toker. 2010. Regulation of oxysterol-binding protein Golgi localization through protein kinase D-mediated phosphorylation. *Mol. Biol. Cell.* 21:2327–2337. https://doi.org/10.1091/mbc.e10-02-0090

Nishimura, T., Y. Uchida, R. Yachi, T. Kudlyk, V. Lupashin, T. Inoue, T. Taguchi, and H. Arai. 2013. Oxysterol-binding protein (OSBP) is required for the perinuclear localization of intra-Golgi v-SNAREs. *Mol. Biol. Cell.* 24:3534–3544. https://doi.org/10.1091/mbc.e13-05-0250

Nohturfft, A., M.S. Brown, and J.L. Goldstein. 1998. Sterols regulate processing of carbohydrate chains of wild-type SREBP cleavage-activating protein (SCAP), but not sterol-resistant mutants Y298C or D443N. *Proc. Natl. Acad. Sci. USA.* 95:12848–12853. https://doi.org/10.1073/pnas.95.22.12848

Nohturfft, A., D. Yabe, J.L. Goldstein, M.S. Brown, and P.J. Espenshade. 2000. Regulated step in cholesterol feedback localized to budding of SCAP from ER membranes. *Cell.* 102:315–323. https://doi.org/10.1016/S0092-8674(00)00037-4

Pagliuso, A., C. Valente, L.L. Giordano, A. Filograna, G. Li, D. Circolo, G. Turacchio, V.M. Marzullo, L. Mandrich, M.A. Zhukovsky, et al. 2016. Golgi membrane fission requires the CtBP1-S/BARS-induced activation of lysophosphatidic acid acyltransferase δ. *Nat. Commun.* 7:12148. https://doi.org/10.1038/ncomms12148

Pakdel, M., and J. von Blume. 2018. Exploring new routes for secretory protein export from the *trans*-Golgi network. *Mol. Biol. Cell.* 29:235–240. https://doi.org/10.1091/mbc.E17-02-0117

Peterson, T.R., S.S. Sengupta, T.E. Harris, A.E. Carmack, S.A. Kang, E. Balderas, D.A. Guertin, K.L. Madden, A.E. Carpenter, B.N. Finck, and D.M. Sabatini. 2011. mTOR complex 1 regulates lipin 1 localization to control the SREBP pathway. *Cell.* 146:408–420. https://doi.org/10.1016/j.cell.2011.06.034

Poumay, Y., and M.F. Ronveaux-Dupal. 1985. Rapid preparative isolation of concentrated low density lipoproteins and of lipoprotein-deficient serum using vertical rotor gradient ultracentrifugation. *J. Lipid Res.* 26:1476–1480.

Radhakrishnan, A., L.-P. Sun, H.J. Kwon, M.S. Brown, and J.L. Goldstein. 2004. Direct binding of cholesterol to the purified membrane region of SCAP: mechanism for a sterol-sensing domain. *Mol. Cell.* 15:259–268. https://doi.org/10.1016/j.molcel.2004.06.019

Radhakrishnan, A., Y. Ikeda, H.J. Kwon, M.S. Brown, and J.L. Goldstein. 2007. Sterol-regulated transport of SREBPs from endoplasmic reticulum to Golgi: oxysterols block transport by binding to Insig. *Proc. Natl. Acad. Sci. USA.* 104:6511–6518. https://doi.org/10.1073/pnas.0700899104

Rawson, R.B., R. DeBose-Boyd, J.L. Goldstein, and M.S. Brown. 1999. Failure to cleave sterol regulatory element-binding proteins (SREBPs) causes cholesterol auxotrophy in Chinese hamster ovary cells with genetic absence of SREBP cleavage-activating protein. *J. Biol. Chem.* 274:28549–28556. https://doi.org/10.1074/jbc.274.40.28549

Ridgway, N.D., P.A. Dawson, Y.K. Ho, M.S. Brown, and J.L. Goldstein. 1992. Translocation of oxysterol binding protein to Golgi apparatus triggered by ligand binding. *J. Cell Biol.* 116:307–319. https://doi.org/10.1083/jcb.116.2.307

Rivera, V.M., X. Wang, S. Wardwell, N.L. Courage, A. Volchuk, T. Keenan, D.A. Holt, M. Gilman, L. Orci, F. Cerasoli Jr., et al. 2000. Regulation of protein secretion through controlled aggregation in the endoplasmic reticulum. *Science.* 287:826–830. https://doi.org/10.1126/science.287.5454.826

Rowland, A.A., P.J. Chitwood, M.J. Phillips, and G.K. Voeltz. 2014. ER contact sites define the position and timing of endosome fission. *Cell.* 159:1027–1041. https://doi.org/10.1016/j.cell.2014.10.023

Schindelin, J., I. Arganda-Carreras, E. Frise, V. Kaynig, M. Longair, T. Pietzsch, S. Preibisch, C. Rueden, S. Saalfeld, B. Schmid, et al. 2012. Fiji: an open-source platform for biological-image analysis. *Nat. Methods.* 9:676–682. https://doi.org/10.1038/nmeth.2019

Shinkawa, T., M. Taoka, Y. Yamauchi, T. Ichimura, H. Kaji, N. Takahashi, and T. Isobe. 2005. STEM: a software tool for large-scale proteomic data analyses. *J. Proteome Res.* 4:1826–1831. https://doi.org/10.1021/pr050167x

Simons, K., and E. Ikonen. 1997. Functional rafts in cell membranes. *Nature.* 387:569–572. https://doi.org/10.1038/42408

Simons, K., and J.L. Sampaio. 2011. Membrane organization and lipid rafts. *Cold Spring Harb. Perspect. Biol.* 3:a004697. https://doi.org/10.1101/cshperspect.a004697

Suchanek, M., R. Hynynen, G. Wohlfahrt, M. Lehto, M. Johansson, H. Saarinen, A. Radzikowska, C. Thiele, and V.M. Olkkonen. 2007. The mammalian oxysterol-binding protein-related proteins (ORPs) bind 25-hydroxycholesterol in an evolutionarily conserved pocket. *Biochem. J.* 405:473–480. https://doi.org/10.1042/BJ20070176

Sun, L.-P., L. Li, J.L. Goldstein, and M.S. Brown. 2005. Insig required for sterol-mediated inhibition of Scap/SREBP binding to COPII proteins in vitro. *J. Biol. Chem.* 280:26483–26490. https://doi.org/10.1074/jbc.M504041200

Taoka, M., A. Wakamiya, H. Nakayama, and T. Isobe. 2000. Protein profiling of rat cerebella during development. *Electrophoresis.* 21:1872–1879.

Taoka, M., N. Morofuji, Y. Yamauchi, H. Ojima, D. Kubota, G. Terukina, Y. Nobe, H. Nakayama, N. Takahashi, T. Kosuge, et al. 2014. Global PROTOMAP profiling to search for biomarkers of early-recurrent hepatocellular carcinoma. *J. Proteome Res.* 13:4847–4858. https://doi.org/10.1021/pr500262p

van Galen, J., F. Campelo, E. Martínez-Alonso, M. Scarpa, J.Á. Martínez-Menárguez, and V. Malhotra. 2014. Sphingomyelin homeostasis is required to form functional enzymatic domains at the trans-Golgi network. *J. Cell Biol.* 206:609–618. https://doi.org/10.1083/jcb.201405009

Venditti, R., M.C. Masone, L.R. Rega, G. Di Tullio, M. Santoro, E. Polishchuk, I.C. Serrano, V.M. Olkkonen, A. Harada, D.L. Medina, et al. 2019. The activity of Sac1 across ER-TGN contact sites requires the four-phosphate-adaptor-protein-1. *J. Cell Biol.* 218:783–797. https://doi.org/10.1083/jcb.201812021

Wakana, Y., S. Takai, K. Nakajima, K. Tani, A. Yamamoto, P. Watson, D.J. Stephens, H.-P. Hauri, and M. Tagaya. 2008. Bap31 is an itinerant protein that moves between the peripheral endoplasmic reticulum (ER) and a juxtanuclear compartment related to ER-associated Degradation. *Mol. Biol. Cell.* 19:1825–1836. https://doi.org/10.1091/mbc.e07-08-0781

Wakana, Y., J. van Galen, F. Meissner, M. Scarpa, R.S. Polishchuk, M. Mann, and V. Malhotra. 2012. A new class of carriers that transport selective cargo from the trans Golgi network to the cell surface. *EMBO J.* 31:3976–3990. https://doi.org/10.1038/emboj.2012.235

Wakana, Y., J. Villeneuve, J. van Galen, D. Cruz-Garcia, M. Tagaya, and V. Malhotra. 2013. Kinesin-5/Eg5 is important for transport of CARTS

Downloaded from http://rupress.org/jcb/article-pdf/220/1/e202002150/1617891/jcb_202002150.pdf by guest on 06 May 2026

from the trans-Golgi network to the cell surface. *J. Cell Biol.* 202: 241–250. https://doi.org/10.1083/jcb.201303163

Wakana, Y., R. Kotake, N. Oyama, M. Murate, T. Kobayashi, K. Arasaki, H. Inoue, and M. Tagaya. 2015. CARTS biogenesis requires VAP-lipid transfer protein complexes functioning at the endoplasmic reticulum-Golgi interface. *Mol. Biol. Cell.* 26:4686–4699. https://doi.org/10.1091/mbc.E15-08-0599

Weber-Boyvat, M., H. Kentala, J. Peränen, and V.M. Olkkonen. 2015. Ligand-dependent localization and function of ORP-VAP complexes at membrane contact sites. *Cell. Mol. Life Sci.* 72:1967–1987. https://doi.org/10.1007/s00018-014-1786-x

Wilhelm, L.P., C. Wendling, B. Védie, T. Kobayashi, M.P. Chenard, C. Tomasetto, G. Drin, and F. Alpy. 2017. STARD3 mediates endoplasmic reticulum-to-endosome cholesterol transport at membrane contact sites. *EMBO J.* 36:1412–1433. https://doi.org/10.15252/embj.201695917

Wyles, J.P., C.R. McMaster, and N.D. Ridgway. 2002. Vesicle-associated membrane protein-associated protein-A (VAP-A) interacts with the oxysterol-binding protein to modify export from the endoplasmic reticulum. *J. Biol. Chem.* 277:29908–29918. https://doi.org/10.1074/jbc.M201191200

Yabe, D., M.S. Brown, and J.L. Goldstein. 2002a. Insig-2, a second endoplasmic reticulum protein that binds SCAP and blocks export of sterol regulatory element-binding proteins. *Proc. Natl. Acad. Sci. USA.* 99: 12753–12758. https://doi.org/10.1073/pnas.162488899

Yabe, D., Z.-P. Xia, C.M. Adams, and R.B. Rawson. 2002b. Three mutations in sterol-sensing domain of SCAP block interaction with insig and render SREBP cleavage insensitive to sterols. *Proc. Natl. Acad. Sci. USA.* 99: 16672–16677. https://doi.org/10.1073/pnas.262669399

Yang, T., P.J. Espenshade, M.E. Wright, D. Yabe, Y. Gong, R. Aebersold, J.L. Goldstein, and M.S. Brown. 2002. Crucial step in cholesterol homeostasis: sterols promote binding of SCAP to INSIG-1, a membrane protein that facilitates retention of SREBPs in ER. *Cell.* 110:489–500. https://doi.org/10.1016/S0092-8674(02)00872-3

Zewe, J.P., R.C. Wills, S. Sangappa, B.D. Goulden, and G.R. Hammond. 2018. SAC1 degrades its lipid substrate PtdIns4*P* in the endoplasmic reticulum to maintain a steep chemical gradient with donor membranes. *eLife.* 7: e35588. https://doi.org/10.7554/eLife.35588

Downloaded from http://rupress.org/jcb/article-pdf/220/1/e202002150/1617891/jcb_202002150.pdf by guest on 06 May 2026

JCB

Supplemental material

Downloaded from http://rupress.org/jcb/article-pdf/220/1/e202002150/1617891/jcb_202002150.pdf by guest on 06 May 2026

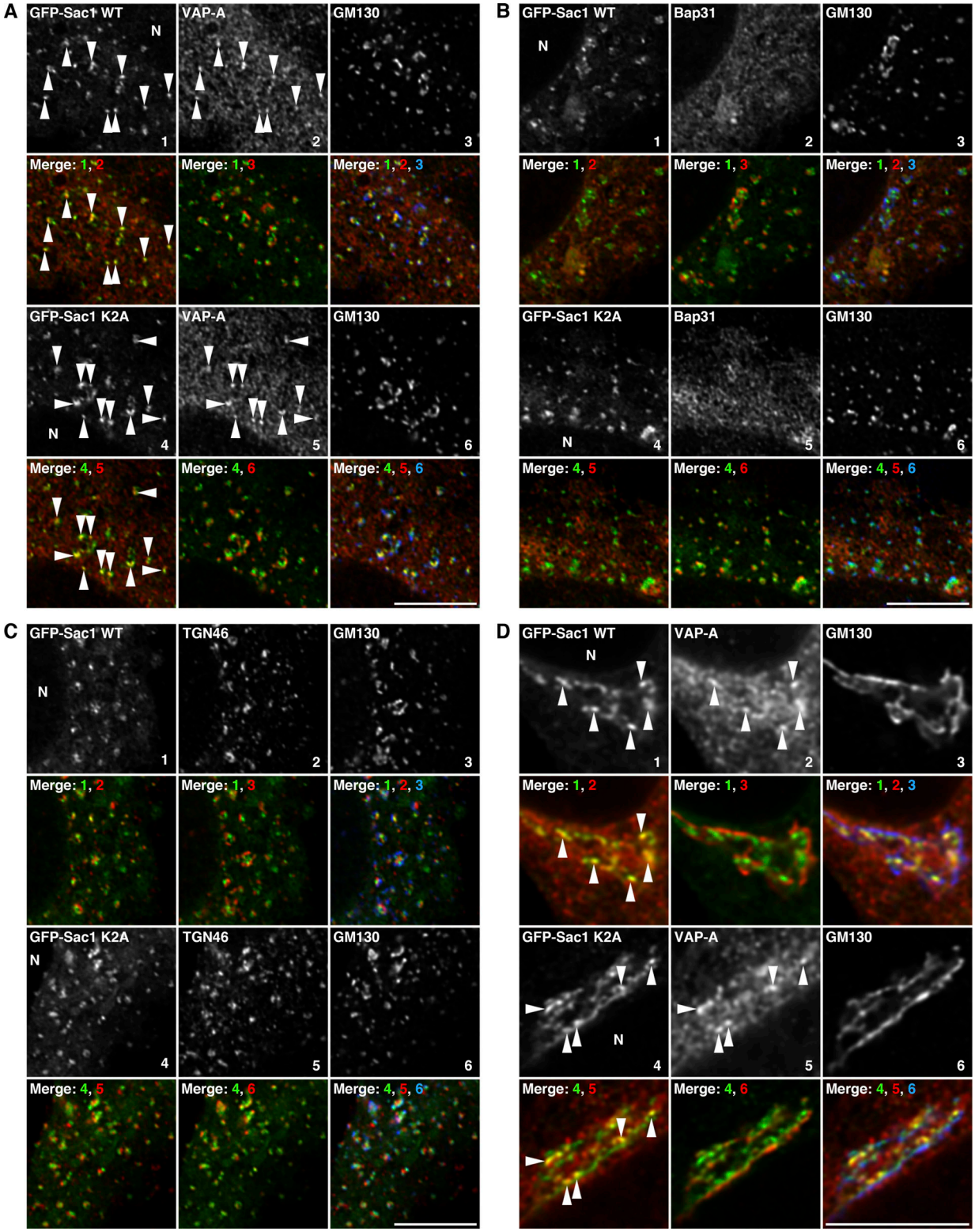

Figure S1. **Colocalization of Sac1 WT or K2A with VAP-A, but not with Bap31, and their proximity to TGN46 or GM130. (A–D)** HeLa cells expressing GFP-Sac1 WT or K2A were treated with 2 µg/ml 25-HC for 1 h with (A–C) or without (D) subsequent treatment with 5 µg/ml nocodazole for 2 h. The cells were fixed and visualized with GFP and antibodies against GM130 and VAP-A (A and D), Bap31 (B), or TGN46 (C). Images were subjected to deconvolution processing as described in Materials and methods. Merged images are shown in the second and fourth rows (second row, left panel: panels 1 and 2 [colored in green and red, respectively]; middle panel: panels 1 and 3 [colored in green and red, respectively]; right panel: panels 1, 2, and 3 [colored in green, red, and blue, respectively]; fourth row, left panel: panels 4 and 5 [colored in green and red, respectively]; middle panel: panels 4 and 6 [colored in green and red, respectively]; right panel: panels 4, 5, and 6 [colored in green, red, and blue, respectively]). Arrowheads indicate the small punctate elements containing both GFP-Sac1 and VAP-A. Scale bars, 10 µm. N, nucleus.

Downloaded from http://rupress.org/jcb/article-pdf/220/1/e202002150/1617891/jcb_202002150.pdf by guest on 06 May 2026

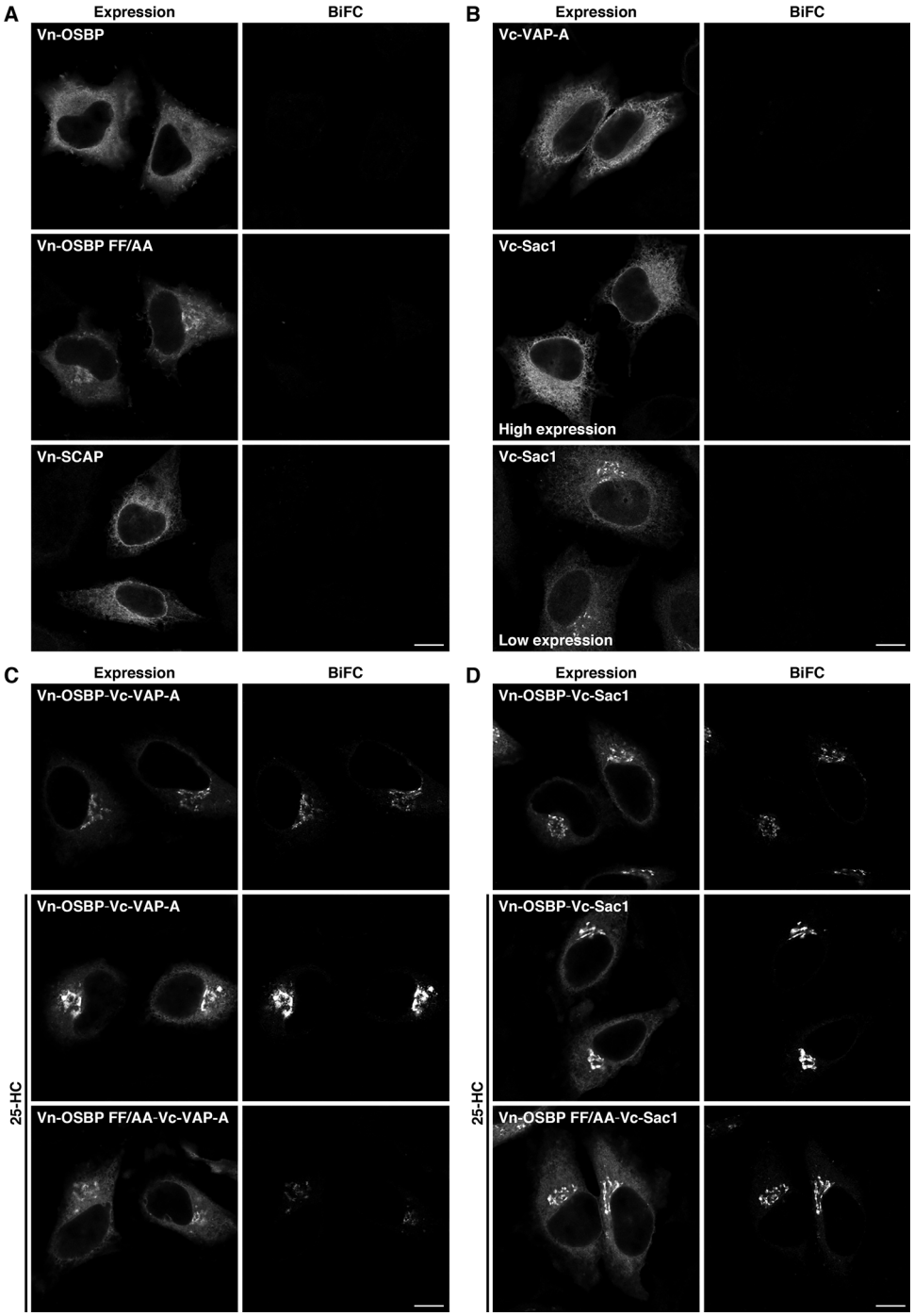

Figure S2. **BiFC visualization of VAP-A, OSBP, and Sac1 interactions at ER–Golgi MCSs. (A and B)** No BiFC signal in HeLa cells with single expression of Vn-fused proteins (A) or Vc-fused proteins (B). **(C and D)** BiFC visualization of OSBP–VAP-A (C) and OSBP–Sac1 (D) interactions at ER–Golgi MCSs. The coexpression of Vn-OSBP WT or FF/AA with Vc-VAP-A (C) or Vc-Sac1 (D) was visualized with an anti-GFP antibody. The BiFC signal was enhanced by treatment of cells with 2 µg/ml 25-HC for 2.5 h. Vn-OSBP FF/AA showed a reduced BiFC signal compared with WT. Scale bars, 10 µm.

Downloaded from http://rupress.org/jcb/article-pdf/220/1/e202002150/1617891/jcb_202002150.pdf by guest on 06 May 2026

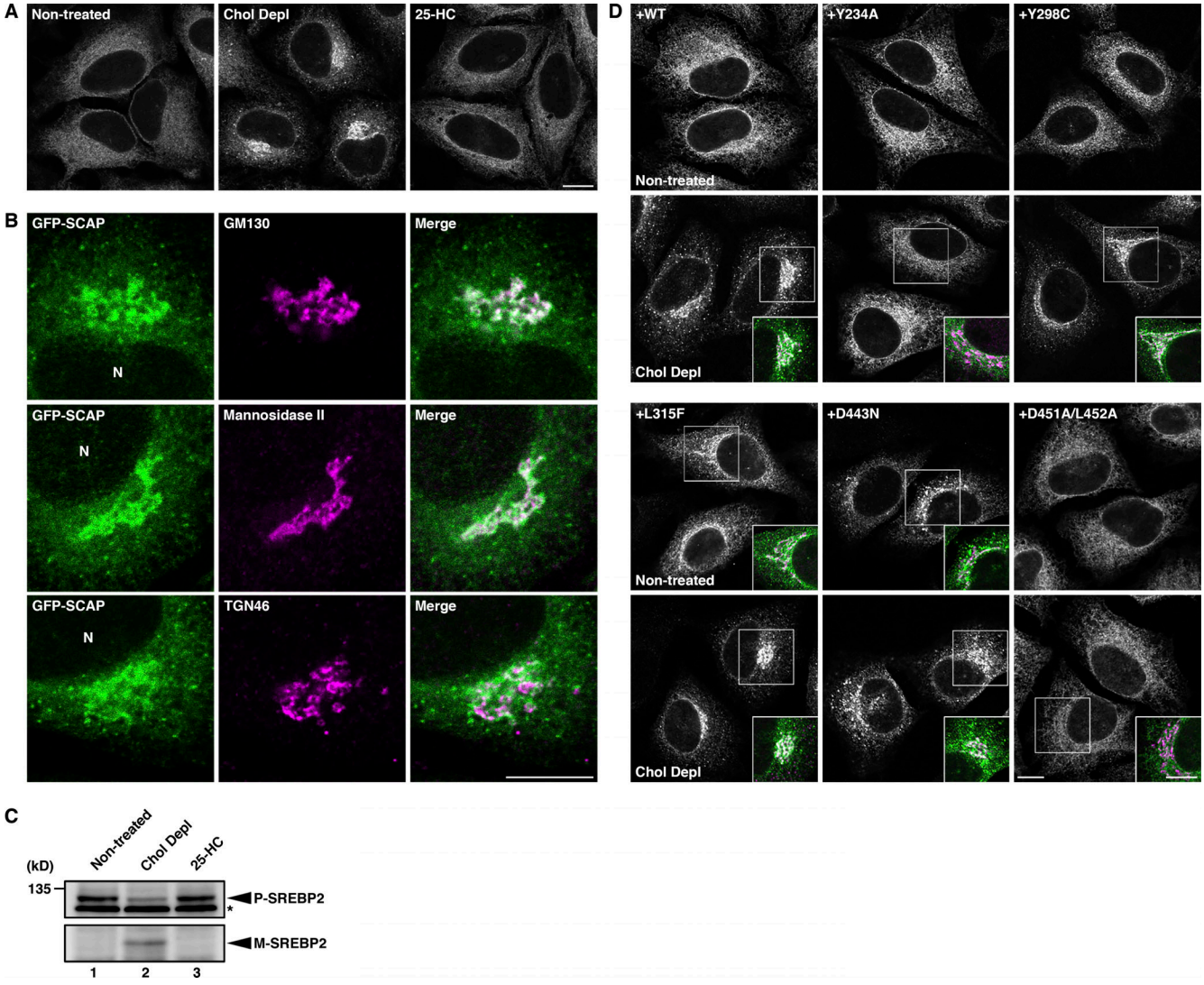

Figure S3. **Sterol-dependent localization of SCAP. (A and B)** Localization of stably expressed GFP-SCAP in HeLa cells with or without cholesterol depletion (Chol Depl) for 3 h or treated with 2 µg/ml 25-HC for 2.5 h. **(B)** Accumulation of GFP-SCAP in GM130 (cis-Golgi matrix protein)– and mannosidase II (cis/medial-Golgi marker enzyme)–positive membranes upon cholesterol depletion. N, nucleus. **(C)** Proteolytic activation of SREBP2 upon cholesterol depletion. Lysates of HeLa cells with or without cholesterol depletion for 3 h or treated with 2 µg/ml 25-HC for 3 h were analyzed by Western blotting with an anti-SREBP2 antibody. Arrowheads indicate the precursor (P) and mature (M) forms of SREBP2. Asterisk denotes nonspecific bands. **(D)** Localization of the stably expressed hamster SCAP WT and mutants in shSCAP HeLa cells with or without cholesterol depletion for 3 h. Merged images for the hamster SCAP WT or mutants (green) and the cis/medial-Golgi marker GPP130 (magenta) of the boxed areas are shown in the insets. Scale bars, 10 µm.

Downloaded from http://rupress.org/jcb/article-pdf/220/1/e202002150/1617891/jcb_202002150.pdf by guest on 06 May 2026

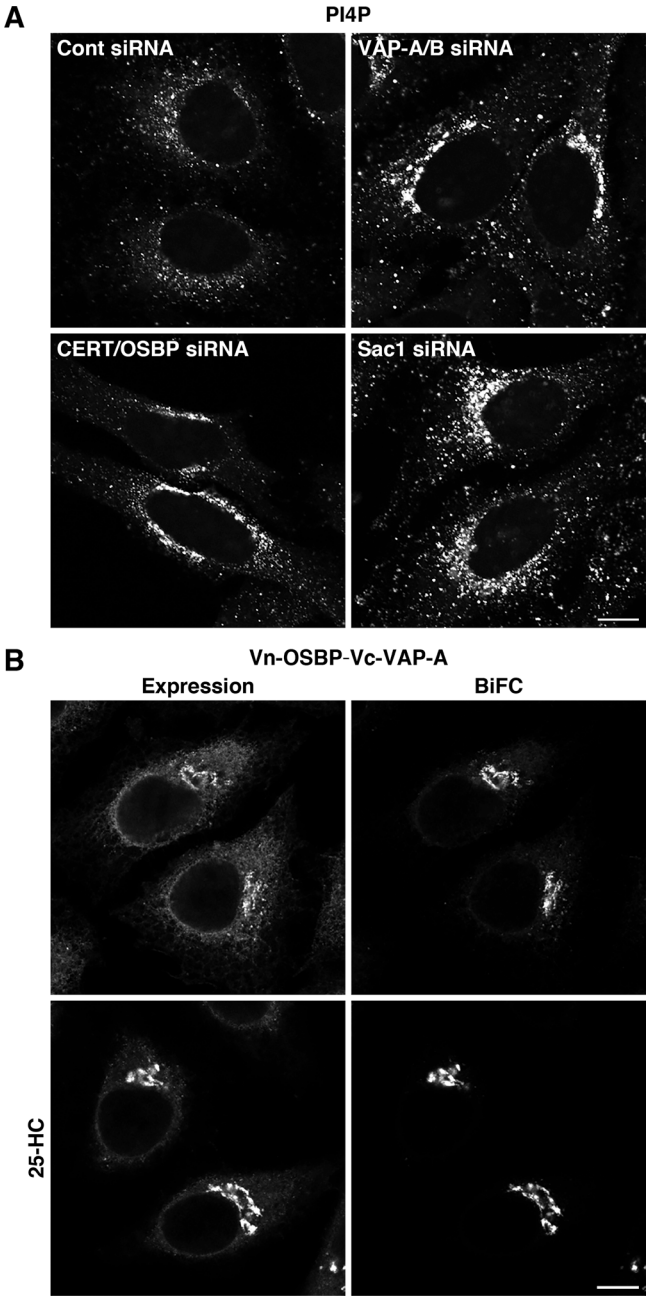

Figure S4. **Effects of knockdown of ER–Golgi MCS components on PI4P turnover and BiFC visualization of the VAP-A–OSBP complex. (A)** PI4P staining in control (Cont), VAP-A/B, CERT/OSBP, and Sac1 knockdown HeLa cells. **(B)** HeLa cells stably coexpressing Vn-OSBP and Vc-VAP-A were treated with or without 2 µg/ml 25-HC for 2.5 h. The coexpression of Vn-OSBP and Vc-VAP-A was visualized with an anti-GFP antibody. Scale bars, 10 µm.

Downloaded from http://rupress.org/jcb/article-pdf/220/1/e202002150/1617891/jcb_202002150.pdf by guest on 06 May 2026

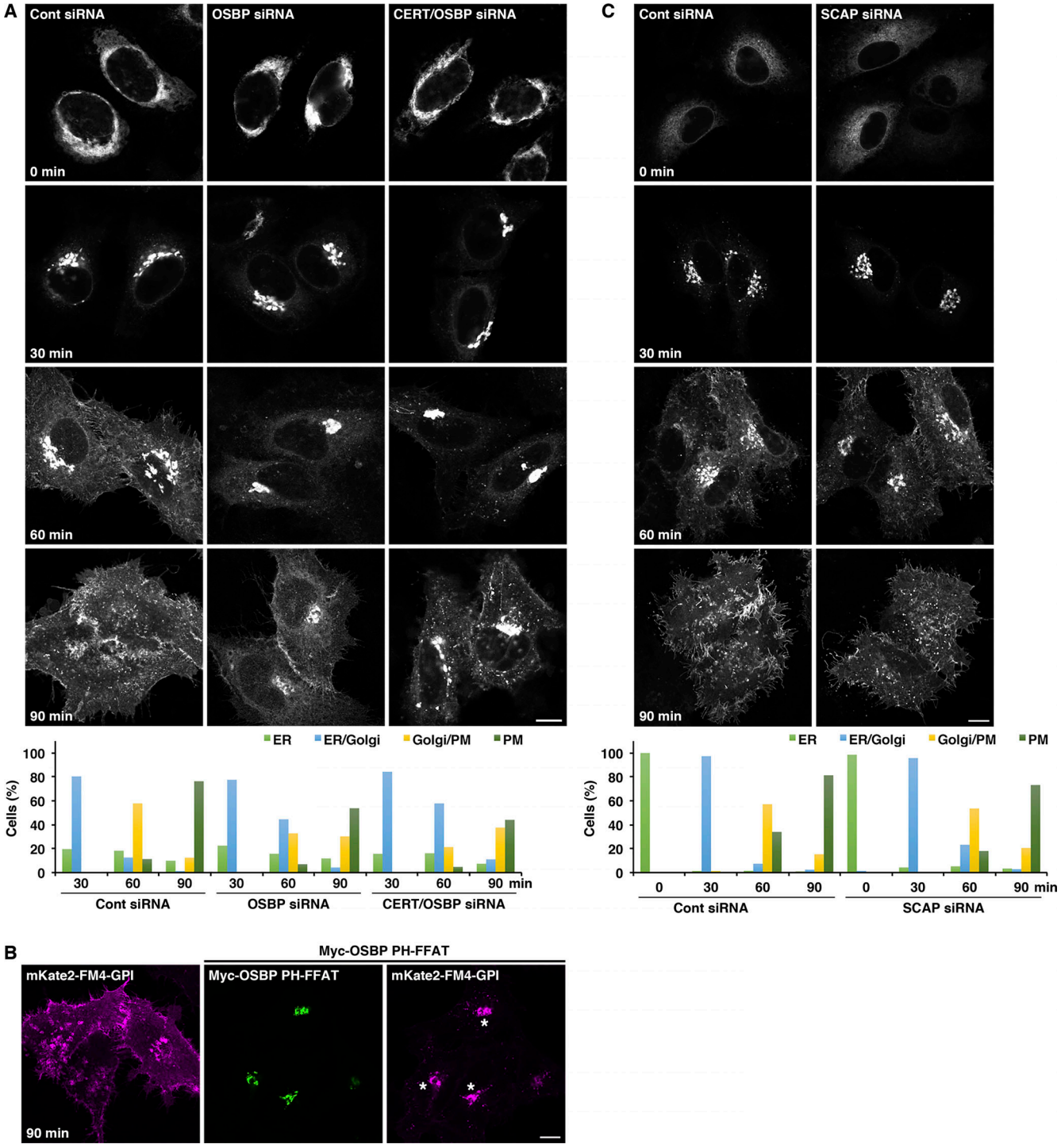

Figure S5. **Effects of knockdown of OSBP, CERT/OSBP, or SCAP on trafficking of GPI-anchored protein or VSV-G. (A)** mKate2-FM4-GPI transport from the ER to the PM via the Golgi complex in control (Cont), OSBP, and CERT/OSBP knockdown cells. The cells were incubated at 37°C with D/D solubilizer and cycloheximide and fixed at the indicated times. The graph shows the percentages of cells with mKate2-FM4-GPI at the ER, ER/Golgi, Golgi/PM, or PM at the indicated times. The data shown are for a single representative experiment out of three performed (n = 229–268 cells per condition). **(B)** mKate2-FM4-GPI transport in the presence or absence of the Myc-OSBP PH-FFAT mutant. Asterisks denote cells coexpressing mKate2-FM4-GPI and Myc-OSBP PH-FFAT. **(C)** VSV-G–GFP transport from the ER to the PM via the Golgi complex in control and SCAP knockdown cells. The cells were incubated at 32°C with cycloheximide and fixed at the indicated times. The graph shows the percentages of cells with VSV-G–GFP at the ER, ER/Golgi, Golgi/PM, or PM at the indicated times. The data shown are for a single representative experiment out of three performed (n = 203–224 cells per condition). Scale bars, 10 µm.

Downloaded from http://rupress.org/jcb/article-pdf/220/1/e202002150/1617891/jcb_202002150.pdf by guest on 06 May 2026

Video 1. **The biogenesis of mKate2-FM4-PAUF–containing CARTS at the TGN.** HeLa cells expressing mKate2-FM4-PAUF were first incubated at 20°C with D/D solubilizer and cycloheximide for 45 min. Images were acquired continuously after the temperature shift to 37°C with a time interval between frames of 30 s for ∼75 min. N, nucleus.

Downloaded from http://rupress.org/jcb/article-pdf/220/1/e202002150/1617891/jcb_202002150.pdf by guest on 06 May 2026